

1   **Impact of battery electric vehicle penetration and corresponding changes in**  
2   **upstream processes on summer O<sub>3</sub> concentrations in Japan**

3   **Satoko Kayaba<sup>1,2</sup> and Mizuo Kajino<sup>2,3</sup>**

4   <sup>1</sup>Graduate School of Science and Technology, University of Tsukuba, Tsukuba, Ibaraki 305-  
5   8572, Japan

6   <sup>2</sup>Meteorological Research Institute (MRI), Japan Meteorological Agency (JMA), Tsukuba,  
7   Ibaraki 305-0052, Japan

8   <sup>3</sup>Faculty of Life and Environmental Sciences, University of Tsukuba, Tsukuba, Ibaraki 305-8572,  
9   Japan

10

11   Corresponding author: Satoko KAYABA (satoko@mri-jma.go.jp)

12

13   **Key Points:**

- 14   • The impact of BEV penetration on summer O<sub>3</sub> concentrations in the Kanto region of  
15   Japan was evaluated
- 16   • Daytime O<sub>3</sub> decreased in both urban and inland suburban areas
- 17   • Additional NO<sub>x</sub> emission from power plants due to night charging for BEV affected next  
18   day daytime O<sub>3</sub> depending on meteorological conditions

19     **Abstract**

20         A regional meteorology–chemistry model was used to assess the effects of passenger car  
21 conversion to battery electric vehicles (BEV) on summer O<sub>3</sub> concentrations in Kanto (Japan's  
22 most populous region). Four sensitivity experiments were conducted on different on-road and  
23 upstream (power plant and gas station) emission conditions. Daytime 8-h maximum O<sub>3</sub>  
24 decreased by 3 ppb (5%) and 4 ppb (5%) in urban and inland suburbs, respectively. O<sub>3</sub> levels  
25 decreased even in urban (VOC-limited regions) because exhaust and evaporative VOC emissions  
26 from vehicle and gas stations were reduced effectively (especially alkenes from gasoline  
27 evaporation; highly reactive in O<sub>3</sub> formation). In the suburbs (NO<sub>x</sub>-limited regions), reduction of  
28 exhaust NO<sub>x</sub> by BEV shifting was significant, but in urban, even only evaporation measures  
29 induced almost the same O<sub>3</sub> reduction effect as BEV shifting. The additional emissions from  
30 thermal power plants due to BEV night charging contributed little to the next day's daytime O<sub>3</sub>  
31 on a monthly average basis. However, on some days, pollutants were stored in the upper part of  
32 the stable nighttime boundary layer and could affect the surface O<sub>3</sub> as the next day's mixed layer  
33 development. Depending on the O<sub>3</sub> sensitivity regime (NO<sub>x</sub>- or VOC-limited), additional NO<sub>x</sub>  
34 plumes from rural (urban) power plants tended to increase (decrease) the next day's O<sub>3</sub>. However,  
35 the distribution of the regime changes temporally and spatially. The H<sub>2</sub>O<sub>2</sub>/HNO<sub>3</sub> ratio was  
36 discovered to be a clear indicator for distinguishing regime boundaries and was effective in  
37 predicting positive or negative O<sub>3</sub> sensitivity to the additional emissions from power plants.

38

39

40    **1      Introduction**

41       Ozone ( $O_3$ ) in surface air has adverse effects on human health, particularly in the  
42      respiratory system (e.g., *Tager et al.*, 2005; *Zhang et al.*, 2019).  $O_3$  is not only an oxidizing agent  
43      by itself, but it also generates strong secondary oxidants such as ascorbic acid ozonide (AOZ)  
44      when degraded by antioxidants in the body (*Tang et al.*, 2007; *Enami et al.*, 2008). Furthermore,  
45      water-soluble gaseous pollutants such as  $SO_2$  influence only the upper respiratory tract, whereas  
46       $O_3$  reaches deep into the lungs because of its hydrophobic nature (*Schraufnagel et al.*, 2019).

47        $O_3$  concentration increases with the coexistence of its precursors,  $NO_x$  ( $NO + NO_2$ ), and  
48      volatile organic compounds (VOCs). VOCs are often referred to as nonmethane VOCs  
49      (NMVOCs) because the reactivity of methane to produce  $O_3$  is much lower compared to that of  
50      other VOCs in urban atmospheres. In Japan,  $NO_x$  and VOC emissions and atmospheric  
51      concentrations continue to plummet and the trend of  $O_3$  concentration has been flat recently after  
52      a period of reduction (*Ito et al.*, 2021). A factor is the reduction ratio of  $NO_x$  to VOCs. For  
53      example, if the rate of VOC reduction is lower than that of  $NO_x$  in a VOC-limited region, such as  
54      an urban area,  $O_3$  may not reduce or could increase.

55       Vehicle transport is one of the major sources of  $O_3$  precursors, but exhaust emission  
56      levels have been reduced to approximately 1/100 of those in the 1960s, before the introduction of  
57      exhaust gas regulations in Japan (*CEC*, 2022). This has been achieved by technological  
58      innovations such as three-way catalysts and diesel particulate filters and by the efforts of  
59      manufacturers. Alternatively, the regulations for fuel evaporation VOCs are less stringent in  
60      Japan than in the United States and European countries (*Uchida*, 2016; *Tonokura and Hata*,  
61      2020). Evaporative VOCs from the automotive-related sectors come from four sources: running  
62      loss (RL), hot soak loss (HSL; caused by leakage from pipes within an hour after stopping),  
63      diurnal breathing loss (DBL; caused by the pressure difference in the tank due to changes in  
64      outside temperature during long periods of parking), and fuel evaporation during refueling.  
65      These evaporative emissions are not associated with diesel but are remarkable for highly volatile  
66      gasoline fuel. In Japan, there are no regulations for RL, whereas in the United States, there are  
67      regulations for RL. HSL and DBL regulations have been introduced, but the time of testing  
68      differs among countries. For example, in the United States, Europe, and China, the DBL emitted

69 during 48 h is measured, whereas in Japan, it is measured during 24 h (*Uchida, 2016*). Onboard  
70 Refueling Vapor Recovery (ORVR) on the vehicle side and Stage 1 (unloading tanks) and Stage  
71 2 (supplying fuel) on the service station side are two measures to prevent fuel evaporation during  
72 refueling. In Japan, no regulation has been introduced for either the vehicle side or the service  
73 station side (Stage 1 is widely used in some prefectures). Although VOC emissions from  
74 stationary sources have been decreasing, emission reductions from service stations have not  
75 progressed as much as those from other sources and their relative contribution is increasing  
76 (*CEC, 2017*).

77 Battery electric vehicles (BEVs) are expected to become more prominent in the future.  
78 This will lead to changes in emissions not only from vehicle exhaust but also from fuel  
79 evaporation and upstream processes. BEVs have zero emissions of exhaust and fuel evaporation  
80 VOCs on-road, but they increase NO<sub>x</sub> emissions from thermal power plants if not charged with  
81 renewable energy. Alternatively, VOC evaporation from gas stations will be reduced because of  
82 reduced fueling opportunities. The impact of vehicle electrification on O<sub>3</sub> concentrations has  
83 been evaluated in the United States (*Thompson, 2009; Nopmongcol et al., 2017; Pan et al.,*  
84 *2019; Schnell et al., 2019*), Spain (*Soret et al., 2014*), China (*Ke et al., 2016*), Taiwan (*Li et al.,*  
85 *2016*), and Japan (*Hata and Tonokura, 2019*). Most of them reported a similar result that the  
86 BEV penetration decreased O<sub>3</sub> concentrations in suburban areas (generally NO<sub>x</sub>-limited regions)  
87 while increasing them in some urban areas and along roadsides (generally VOC-limited regions).  
88 *Nopmongcol et al. (2017)* demonstrated the results of O<sub>3</sub> reduction in Los Angeles, an urban area,  
89 but this assumed that off-road vehicles are also electrified, which contributed to VOC emission  
90 reduction. *Hata and Tonokura (2019)* evaluated the impact of hybrid electric vehicle or zero-  
91 emission vehicle (ZEV) penetration in Japan on summer O<sub>3</sub> concentrations. They reported that  
92 converting all vehicles (including trucks and buses) to ZEVs increased O<sub>3</sub> levels in urban centers.  
93 However, if only passenger cars were converted to ZEVs, daytime O<sub>3</sub> levels in urban centers  
94 decreased.

95 The results of these previous studies indicate that the O<sub>3</sub> sensitivity of BEV penetration  
96 depends on the following: “baseline emission of NO<sub>x</sub> and VOCs in the target area (which are  
97 affected by other sources and emission controls),” “reduction ratio of NO<sub>x</sub> and VOCs,” and “O<sub>3</sub>  
98 sensitivity regime (NO<sub>x</sub>- or VOC-limited) in the target area.” Only a few of the previous studies  
99 have examined emission changes in upstream processes. *Hata and Tonokura (2019)* considered

100 emission changes from fueling stations but did not consider emission changes from power plants.  
101 In this study, we evaluated the impact of passenger car BEV shift on summer O<sub>3</sub> concentrations  
102 in Japan using a regional meteorology–chemistry model while accounting for upstream (power  
103 plant and gas station) emission changes.

104 Section 2 describes the methodology, including an overview of the CTM, observation  
105 data for model evaluation, and the sensitivity experiment assumptions. Section 3 contains the  
106 results and discussion of the model evaluation, the impact of BEV penetration on O<sub>3</sub>  
107 concentrations, and the impact of additional power plant emissions for BEV charging on O<sub>3</sub>  
108 concentrations. Section 4 finally discusses the conclusions and future works.

109 **2 Materials and Methods**

110 **2.1 Regional meteorology–chemistry model**

111 A regional-scale nonhydrostatic meteorology–chemistry model (NHM-Chem) (*Kajino et al., 2019; Kajino et al., 2021*) was used in this study. Detail descriptions are summarized in  
112 Table S1.

114 **Figure 1** shows the model calculation domain in this study. The mother domain (domain  
115 01) covered the Northeast Asian region and was calculated with dx = 30 km. The nested domain  
116 (domain 02) covered the Japanese region from Kyushu to Tohoku and was calculated with dx = 6  
117 km. The vertical layer was 40 layers up to an altitude of approximately 20 km in both domains.  
118 Subsequently, model results refer to mixing ratios at the lowest level (approximately 15 m above  
119 ground level) unless altitude is specifically mentioned. The target period of this study was from  
120 July 1 to 31, 2015, and the simulations were integrated from June 26, with a spin-up period of  
121 five days. Summer is a season with the highest O<sub>3</sub> concentrations observed in Japan due to high  
122 solar radiation. Furthermore, the contribution of transboundary transport from East Asia is  
123 relatively low in summer compared to spring, so the contribution of domestic sources is high.  
124 Therefore, July was chosen as the target period because the O<sub>3</sub> concentration is considered the  
125 most sensitive to BEV penetration in Japan.

126 We used REASv3.2.1 (minor revision in December 2021 from v3.2 (*Kurokawa and Ohara, 2020*), 0.25° × 0.25°, base year = 2015) for anthropogenic emission for Northeast Asia  
127 and PM2.5EI (*Morikawa, 2017*, 1 km × 1 km, base year = 2012) for Japan. The NO<sub>x</sub> emissions  
128 were allocated 9:1 to NO and NO<sub>2</sub> for both REASv3.2.1 and PM2.5EI. The VOC speciation of

130 REASv3.2.1 was recategorized to those of the chemical reaction mechanism (SAPRC99; *Carter*,  
131 *2000*) for both REASv3.2.1 and PM2.5EI. PM2.5EI is excellent in its detailed categorization and  
132 estimation of vehicle emissions. Emissions were estimated using statistical data of traffic volume  
133 and average vehicle speed by the time of day and weekday/weekend. Furthermore, emissions  
134 were estimated for 120 categories, combining eight vehicle types (mini passenger car, passenger  
135 car, bus, light-duty truck, heavy-duty truck, special use truck, and motorcycle), five emission  
136 processes (running, start, RL, HSL and DBL), and three fuel types (gasoline, diesel, and LPG).  
137 At the smokestack altitude, power plants release pollutants. Taking chimney elevation into  
138 account, emissions from industries and power plants were distributed in this study from 0 to 300  
139 m above the ground level. For domain 1 with Japan and domain 2 without Japan, REASv3.2.1  
140 was used (i.e., Korea). For domain 2 over Japan, PM2.5EI was used. EAGrid (*Fukui et al.*, 2014;  
141 *Kannari et al.*, 2007) was used instead because ship emissions are not available in PM2.5EI.  
142 GFED v4 (*Giglio et al.*, 2013) was used for biomass burning emissions, and JMA observation  
143 data were used for volcanic SO<sub>2</sub> emissions. Biogenic VOC emissions were inline calculated  
144 based on MEGAN v2 (*Guenther et al.*, 2006) as a function of temperature and solar radiation.

145 For the initial and boundary conditions for the NHM (meteorological model part of  
146 NHM-Chem), we used a 6-hourly JRA-55 global reanalysis dataset (*Kobayashi et al.*, 2015) for  
147 domain 01 and 3-hourly JMA's Meso-Regional Objective Analysis (MA) for domain 02  
148 (<https://www.jma.go.jp/jma/jma-eng/jma-center/nwp/nwp-top.htm>, last accessed: 30 July 2022).  
149 Spectral nudging above a height of 7 km was applied for the large-scale wave components of  
150 horizontal momentum and potential temperature (wavelength > 1,000 km), with a weighting  
151 factor of 0.06. For the chemical transport model (CTM) part of NHM-Chem, monthly  
152 climatological values were used for the initial and boundary concentrations of domain 01 and the  
153 results of domain 01 were used for domain 02. The input/output time interval of CTM was 1 h.

## 154 2.2 Model experimental cases and parameter settings

### 155 2.2.1 Emission scenarios

156 As shown in *Table 1*, four model experiments (or emission scenarios) were conducted in  
157 this study. Heavy-duty vehicles and motorcycles were assumed to be nonelectric. The  
158 assumptions of total vehicle ownership and activity were not changed in the sensitivity  
159 experiment to evaluate the sensitivity to changes in emission factors.

160 (1) “BASE” experiment

161 This is a replicated experiment of the current situation based on the meteorological field in 2015.

162 Emissions are based on each inventory (Table S1).

163 (2) “All BEV” experiment

164 All passenger cars are shifted to BEVs. All BEV charging is conducted at night (23:00–8:00) to  
165 level out demand. During this period, additional emissions from thermal power plants are  
166 produced.

167 (3) “All BEV (PP unchanged)” experiment

168 All passenger cars are shifted to BEVs, with power plant (PP) emissions unchanged (assumed  
169 100% supplied by renewable energies). The difference between (2) and (3) indicates the  
170 sensitivity of additional power plant emissions.

171 (4) “Evapo reduce” experiment

172 Only evaporative NMVOCs emitted by passenger vehicles and gas stations are reduced  
173 (passenger car exhaust remains unchanged). This is the situation when only evaporation  
174 measures are conducted without BEV penetration.

175

## 176 2.2.2 Changes in upstream emissions due to BEV penetration

177 Figure S1 demonstrates the diurnal additional electricity demand for BEV charging. We  
178 assumed normal nighttime charging for all BEVs because a large percentage of BEV users  
179 currently charge late-night electricity at home (*MLIT urban bureau, 2012*). The load due to  
180 increased demand is assumed to be charge-controlled to level out. Thermal power plant  
181 emissions increase during the 9 h period (from 23:00 to 8:00). The increased electricity demand  
182 for BEV charging is derived to be 71.4 billion kWh/year, assuming an average electricity  
183 consumption of 0.17 kWh/km for BEVs and a total annual passenger car travel volume of 420  
184 billion km/year (*MLIT, 2010*). This increased demand corresponds to approximately 7% of total  
185 electricity demand (1077.8 billion kWh/year), which will be met by nighttime baseload and  
186 middle power (90% thermal and 10% hydro in 2012, the base year for the PM2.5EI). The  
187 emissions from the thermal power plant for this 9 h period would increase by approximately  
188 25%–30%, assuming that plant emissions are proportional to the amount of electricity generated.  
189 In reality, emissions will not increase proportionately with the increased generation because

190 generation efficiency will increase. However, in the same manner, as in previous studies  
191 (*Thompson et al., 2011; Soret et al., 2014; Ke et al., 2016; Li et al., 2016; Schnell et al., 2019*),  
192 we assumed proportional to this study because no information regarding the relationship among  
193 power generation, generation efficiency, and emissions was available. The power grid in Japan is  
194 assumed to be uniform. In reality, LNG-fired power would be applied as the marginal power, but  
195 coal, oil, and LNG-fired power were assumed to increase uniformly.

196 The evaporation NMVOCs is assumed to be reduced by 80% because BEV penetration  
197 will reduce refueling frequency. Here 80% is the share of gasoline consumption by passenger  
198 cars to that of total (*MLIT, 2012*). Although emission changes at refineries should be considered  
199 as well as power plants and gas stations, it was assumed to be unchanged in this study. Because  
200 estimating the change in crude oil refining volume is difficult (not only gasoline demand but also  
201 other petroleum products will be involved).

202

### 203 2.3 Observation data for model validation

204 The Ministry of the Environment, Japan (MOEJ)'s wide area monitoring data for air  
205 pollutants (Atmospheric Environmental Regional Observation System: AEROS) were used to  
206 validate the simulation results of O<sub>3</sub> concentrations. The concentrations of SO<sub>2</sub>, NO, NO<sub>2</sub>, Ox,  
207 CO, NMHC, CH<sub>4</sub>, THHC, SPM, and PM<sub>2.5</sub> are monitored hourly every day at approximately  
208 1900 measuring stations throughout Japan (some substances are not measured at some stations).  
209 The National Institute for Environmental Studies screens out anomalous data from those  
210 preliminary values and publishes confirmed data. Confirmed data were used in this study. We  
211 generated super observation data by simply averaging the hourly observation data of observation  
212 sites in each model grid (dx = 6 km) to compare against the simulation results. In the Kanto  
213 region, there are 234 super observation grids.

214

215

216 **3 Results and Discussion**217 **3.1 Model evaluation**

218 Comparative statistics between the model BASE experiment and observations with daily  
219 average O<sub>3</sub> and MDA8h O<sub>3</sub> (daily maximum 8 h average O<sub>3</sub>) are shown in [Table 2](#). The top two  
220 rows are the Kanto area ([Figure 1](#)) averaged data for 31 days. The correlation coefficients of  
221 these data indicate day-by-day temporal correlations because the diurnal variation of O<sub>3</sub> is  
222 smoothed out. The correlation coefficients are higher for both daily average O<sub>3</sub> and MDA8h O<sub>3</sub>  
223 (R = 0.66 and 0.79, respectively), indicating that the model accurately reproduced the temporal  
224 variability of daily high concentration events affected by weather conditions. The bottom two  
225 rows are July monthly averaged data for the nationwide 864 super observation grids (all of  
226 domain 2, [Figure 1](#)). The correlation coefficients of these data indicate the spatial correlations.  
227 They show a moderate correlation (R = 0.32 and 0.56 for daily average O<sub>3</sub> and MDA8h O<sub>3</sub>,  
228 respectively). This is because the highest O<sub>3</sub> concentration was distributed in Kanto inland in the  
229 model's result, whereas in the observation data, it was distributed in Kyushu and Chugoku.  
230 However, within only Kanto (N = 234), the correlation coefficient was higher (R = 0.6). The  
231 model reproduced the distribution of the O<sub>3</sub> concentration gradient from the coastal to the inland  
232 areas of the Kanto region relatively well.

233 The simulated MDA8h O<sub>3</sub> over Kanto was slightly overestimated (NMB = 3.6%)  
234 probably because of the overestimation of photochemical production. Alternatively, the  
235 simulated daily average O<sub>3</sub> concentration is slightly underestimated (NMB = -9.7%) probably  
236 because of a slight overestimation of the nighttime NO titration ([Figure S2](#)).  
237

238 **3.2 Impact of passenger cars shifting to BEVs on daytime O<sub>3</sub> concentration**239 **3.2.1 Results of passenger car “all BEV” experiments**

240 [Figure 2](#) shows NO<sub>x</sub> and NMVOC emissions in the BASE experiment ([Figure 2a, d](#)) and  
241 their change with the shift of all passenger cars to BEVs (i.e., (2) All BEV experiment — (1)  
242 BASE experiment). [Figure 3](#) shows the diurnal variation of these emissions in major sources

(Figure 2 area (A)). The industry sector is the largest NO<sub>x</sub> emission source, followed by heavy-duty vehicles during the daytime. The contribution of passenger car emissions was low (Figure 3a). NO<sub>x</sub> emission was reduced by up to 10%–15% by BEV shifting during urban commuting hours (Figure 2b), that is, approximately –5% during daytime area (A) average (Figure 3b). It increases approximately 5% net for the nighttime area (A) average (Figure 3b). At night, emissions increase from thermal power plants, and they decrease from passenger cars, but the effect is small because of low traffic volumes (Figure 2c).

Although higher biogenic NMVOC emissions in July, anthropogenic NMVOC emissions accounted for approximately 90% of total NMVOC emissions in urban areas (Figure 2e). It is mainly from stationary sources such as the painting industry (Figure 3c). The NMVOC emission was reduced by approximately 10% by BEV shifting for the area (A) average (Figure 3d), owing to a reduction in three sources: passenger car exhaust, passenger car evaporation, and gas station evaporation.

Figure 4a shows the July average of MDA8h O<sub>3</sub> concentrations in the BASE experiment. High O<sub>3</sub> concentration is distributed inland along the topography is because precursors emitted in the urban coastal areas are transported by sea breezes (e.g., *Ooka et al.*, 2011). The MDA8h O<sub>3</sub> sensitivity by BEV shifting was also large inland, with a maximum of approximately –5 ppb (–5%) (Figure 4b).

Figure 4c shows the MDA8h O<sub>3</sub> sensitivity when only fuel evaporation measures for passenger cars and gas stations are taken (i.e., (4) Evapo reduce experiment — (1) BASE experiment). The reduction rate is almost the same as that in Figure 4b even without reducing vehicle exhaust in Tokyo and the southern part of Saitama because these areas are VOC-limited regions. Because there is a time lag before BEVs are widely spread in the real world, it is effective to implement ahead with fuel evaporation measures to reduce urban O<sub>3</sub>. Specifically, Stage 2 (add a gas recovery system to the refueling pump and return it to an underground tank) and ORVR (add a gas adsorption system with activated carbon sealed to the vehicle) are the main measures during refueling. Changing the rubber material of the vehicle pipe to one that is less permeable and increasing the capacity of the gas adsorption system are the main parking measures. Among these, Stage 2 is estimated to be cost-effective (CEC, 2017). Furthermore, the effect of Stage 2 in reducing summer O<sub>3</sub> concentration in Kanto was demonstrated using an atmospheric model (*Nakagawa et al.*, 2019). Therefore, it is considered an effective measure.

274 Conversely, it was also suggested that reducing NO<sub>x</sub> emissions in urban areas is  
275 important to reduce high concentrations of O<sub>3</sub> inland (NO<sub>x</sub>-limited region) and that BEV  
276 penetration can benefit from this (Figure 4b, c).

277

278       3.2.2 O<sub>3</sub> formation potential of NMVOCs

279       The reactivity of NMVOCs for O<sub>3</sub> formation varies according to species. In this section,  
280 we quantify the relative contributions of species and sources to the reduction of O<sub>3</sub>, as presented  
281 in Section 3.2.1.

282       Figure 5a depicts the emissions of NMVOCs in Area (A) (Figure 2) as well as the amount  
283 of reduction due to BEV shift. Figure 5b depicts the breakdown of the contribution of each  
284 species and source to the reduction. The NMVOC composition of exhaust and gasoline fuel  
285 evaporation is shown in Figure S3. The composition of gasoline and diesel exhaust gas  
286 components is based on data from a tunnel survey conducted in Tokyo in 2010 (*Uchida et al.*,  
287 2013). The gasoline vehicle exhaust was dominated by alkanes (approximately 50%), followed  
288 by aromatics (approximately 40%) and alkenes (approximately 9%) (Figure S3a). The NMVOC  
289 composition of gasoline fuel evaporation is based on data from the DBL test (*Yamada et al.*,  
290 2015a). The species from permeation (leak gas from the rubber pipe of the vehicle) are alkanes  
291 (55%), aromatics (25%), and alkenes (20%) (Figure S3c). Alternatively, the species from  
292 breakthrough (leak evaporative gas in the fuel tank when over the capacity of the canister) are  
293 alkanes (68%) and alkenes (32%) and do not include aromatics (*Yamada et al.*, 2015a) (Figure  
294 S3d). This is because species with low molecular weight and high volatility dominate in  
295 evaporative gas in the tank (*Hagino et al.*, 2015). Permeation species predominate in RL, HSL,  
296 and the first day of DBL, whereas breakthrough species predominate after the second day of  
297 DBL (*Yamada et al.*, 2015a; *Hagino et al.*, 2015). Therefore, in this study, permeation data from  
298 the DBL test are adopted for RL and HSL and breakthrough data are adopted for DBL.

299       The composition of refueling evaporation is also composed of alkanes (75%) and alkenes  
300 (23%), as shown in Figure S3e (*Yamada et al.*, 2015b). It lacks aromatics for the same reason  
301 that a breakthrough does. Additionally, the test by *Yamada et al.* (2015a and 2015b) was  
302 conducted under 20°C conditions. However, it has been reported that the NMVOC composition

303 of refueling evaporative gas remained unchanged when the temperature was increased from 10°C,  
 304 25°C, to 30°C (*Hagino et al., 2015*).

305 The emissions of NMVOC mass were reduced by approximately 10% in Area (A) by  
 306 BEV shifting (*Figure 5a*). The most reduced of these was alkane (65% contribution). By the  
 307 source, passenger car exhaust gas, passenger car fuel evaporation, and gas station fuel  
 308 evaporation contributed roughly 4:3:3 to the mass reduction of NMVOCs (*Figure 5b*).

309 *Figures 5c* and *5d* are the same as *Figures 5a* and *5b* but for ozone formation potential  
 310 (OFP), which considers the reactivity of each NMVOC species. OFP is derived by Equation (1),  
 311 which is calculated by weighting NMVOC emissions by MIR, the reactivity index of O<sub>3</sub>  
 312 production.

313

314 
$$OFP_i = E_i \times MIR_i, \quad (1)$$

315

316 where *OFP<sub>i</sub>* is the O<sub>3</sub> formation potential of NMVOC species i (g-O<sub>3</sub> h<sup>-1</sup>), *E<sub>i</sub>* is the emission of  
 317 NMVOC species i (g-NMVOC h<sup>-1</sup>), and *MIR<sub>i</sub>* is the maximum incremental reactivity of  
 318 NMVOC species i (g-O<sub>3</sub>/g-NMVOC). The MIR values are displayed in Table S2, which are  
 319 based on *Carter* (2000). *Carter* (2000) derived these MIR values by conducting sensitivity  
 320 experiments using the box model of the SAPRC-99 chemical module.

321 The OH reaction rate constant (kOH) (*Atkinson, 1994; Atkinson, 1997; Atkinson, 2000*) is  
 322 an index for comparing the reactivity of NMVOC species. Although MIR was employed in this  
 323 study because MIR is superior in that it can consider the effects of secondary reactions, which  
 324 kOH cannot. More specifically, kOH represents only the initial OH reactivity in the RO<sub>x</sub> cycle  
 325 and cannot account for differences in reactivity between RO<sub>2</sub> and NO produced after that. As a  
 326 result, there is a concern that it overestimates the impact of NMVOC species that react quickly  
 327 with OH but do not produce a significant amount of O<sub>3</sub> in subsequent reactions (or vice versa)  
 328 (*Carter, 1994; Tajima et al., 2010*).

329 The OFP decreased approximately 5.5% in Area (A) by BEV shifting, slightly less than  
 330 the mass-based reduction (*Figure 5c*). This is due to the lower MIR of alkanes, which contributed  
 331 the most to the mass-based reduction. Instead, the reduction of alkene contributed the most to  
 332 OFP reduction (47% contribution) (*Figure 5d*). The contribution of the three sources was 4:3:3,  
 333 which is consequently the same as mass-based results (*Figure 5d*). Overall, it was estimated that

334 the alkenes from passenger car and gas station fuel evaporation, as well as the aromatics from  
335 passenger car exhaust gases, contributed significantly to the O<sub>3</sub> reduction achieved through BEV  
336 shifting ([Figure 5d](#)). They contributed 19%, 18%, and 13% to OFP reduction, respectively.

337

338

339       3.3 Impact of additional emissions from a thermal power plant due to nighttime BEV  
340           charging on the next day's daytime O<sub>3</sub>

341 Thermal power plants are typically located in coastal areas. A previous study based on BEV  
342 penetration in Spain ascertained that even if BEV charging increased pollutant emissions from  
343 gas-fired power generation at night, nighttime onshore winds would wash the pollutant plume  
344 seaward with no problem ([Soret et al., 2014](#)). As such, the impact of additional power plant  
345 emissions may not affect residential areas. However, there could be a case that the impact is  
346 significant depending on the meteorological field and emission conditions, so we discuss it in  
347 this section. That is, evaluating the impact of additional NO<sub>x</sub>, given that the power plant emits  
348 almost no NMVOCs ([Figure 3c, d](#)).

349       [Figure 6a](#) depicts the sensitivity of July mean MDA8h O<sub>3</sub> concentration due to additional  
350 power plant emissions (i.e., (2) All BEV experiment — (3) All BEV (PP unchanged)  
351 experiment). The areal maximum sensitivity was very low at approximately -0.5% (-0.2 ppbv)  
352 monthly. This is because the advection path of the plume and the daytime photochemical  
353 reaction rate vary depending on the daily wind pattern and solar radiation (as confirmed by the  
354 hourly O<sub>3</sub> sensitivity map).

355       However, there were some cases of relatively high sensitivity. [Figure 6b](#) depicts the case  
356 at 13:00 on July 26. Around Tokyo Bay and Lake Kasumigaura, the O<sub>3</sub> sensitivities are  
357 approximately -5% (-4 ppb) and +5% (+5 ppb) (area enclosed with a solid line). They were  
358 carried by additional plumes from thermal power plants in Tokyo Bay and Kashima city,  
359 respectively. Similar cases of relatively high O<sub>3</sub> sensitivity were discovered over several days in  
360 late July. This may be due to the high solar radiation and temperatures in late July 2015 caused  
361 by the predominance of the Pacific High, which accelerated the photochemical O<sub>3</sub> formation.

362       The positive or negative sensitivity of O<sub>3</sub> to such additional NO<sub>x</sub> depends on whether the  
363 region is NO<sub>x</sub>- or VOC-limited. Generally, the O<sub>3</sub> sensitivity regime is VOC-limited in urban  
364 areas and NO<sub>x</sub>-limited in a suburb (e.g., [Sillman, 1999](#)). This is also the case in the Kanto region

365 of Japan, where the rate changes from VOC-limited to NO<sub>x</sub>-limited as one moves from the urban  
366 center around Tokyo Bay to the inland suburbs (*Inoue et al.*, 2010a). As a result, the positive and  
367 negative O<sub>3</sub> sensitivities enclosed with solid lines are consistent with this trend. However, there  
368 are cases where O<sub>3</sub> has negative sensitivity (i.e., VOC-limited) despite living in a suburban area  
369 (area enclosed with a dashed line).

370 In this section, we first analyze the distribution of NO<sub>x</sub> or VOC sensitivity regimes in  
371 such high O<sub>3</sub> sensitivity cases (Sec. 3.3.1). Then, the mechanism by which additional NO<sub>x</sub> is  
372 emitted from the power plant stack to result in next day sensitivity was analyzed, focusing on the  
373 effect of atmospheric stability (Sec. 3.3.2).

374

375       3.3.1 O<sub>3</sub> sensitivity regime and H<sub>2</sub>O<sub>2</sub>/HNO<sub>3</sub> indicators

376        3.3.1.1 Radical cycle and termination process

377       This section provides a brief description of the O<sub>3</sub> formation mechanism and sensitivity  
378 regime, which will be required for the subsequent discussion. The increase in tropospheric O<sub>3</sub> is  
379 caused by the RO<sub>x</sub> cycle, which is initiated by the oxidation of VOCs by OH. The RO<sub>x</sub> cycle  
380 causes an imbalance of the NO<sub>x</sub> cycle equilibrium (NO<sub>2</sub> + O<sub>2</sub> ⇌ NO + O<sub>3</sub>) and contributes to  
381 NO<sub>2</sub> formation (RO<sub>2</sub> + NO → RO + NO<sub>2</sub>, HO<sub>2</sub> + NO → OH + NO<sub>2</sub>). Under high NO<sub>x</sub> conditions,  
382 the terminal reactions are as follows, producing HNO<sub>3</sub> and PAN.

383



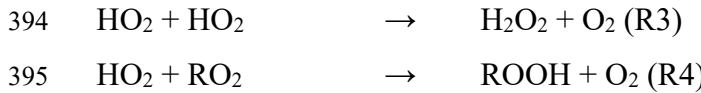
386

387       The additional NO<sub>x</sub> in this situation reduces O<sub>3</sub> because it deprives OH available for VOC  
388 oxidation and inhibits the RO<sub>x</sub> cycle. As a result, the O<sub>3</sub> concentration rises with increasing  
389 VOCs and falls with increasing NO<sub>x</sub>, indicating that the region is a VOC-limited region.

390

391       Alternatively, under low NO<sub>x</sub> conditions, these self-reactions among HO<sub>2</sub> and between  
392 HO<sub>2</sub> and RO<sub>2</sub> are the termination reactions, producing H<sub>2</sub>O<sub>2</sub> and ROOH.

393



396

397   Therefore, the  $\text{O}_3$  concentration is not affected by VOCs but by the  $\text{NO}_x$  concentration,  
 398 indicating that the region is  $\text{NO}_x$ -limited.

399

400   On the basis of the above mechanism, the  $\text{O}_3$  sensitivity in [Figure 6b](#) can be explained by the  
 401    $\text{NO}_x$ ,  $\text{NO}_y$  (all oxidized nitrogen compounds),  $\text{NO}_z$  ( $\text{NO}_y$  minus  $\text{NO}_x$ ), nonmethane hydrocarbons  
 402   (NMHC), and  $\text{NO}_2/\text{NO}_x$  sensitivity as shown in [Figure 7](#). Around Tokyo Bay, the positive  $\text{NO}_x$   
 403   sensitivity brought by the power plant during the night remained until the next daytime ([Figure](#)  
 404   [7a](#)). NMHC sensitivity was positive because the additional  $\text{NO}_x$  inhibited the  $\text{RO}_x$  cycle (=  
 405   suppressed VOC consumption) ([Figure 7d](#)). The  $\text{NO}_2$  formation was suppressed,  $\text{NO}_2/\text{NO}_x$  ratio  
 406   decreased ([Figure 7e](#)), and  $\text{O}_3$  also decreased ([Figure 6b](#)). Alternatively, no  $\text{NO}_x$  sensitivity was  
 407   found around Lake Kasumigaura ([Figure 7a](#)). This is because all  $\text{NO}_x$  was converted to  $\text{NO}_z$   
 408   ([Figure 7c](#)). NMHC sensitivity was negative ([Figure 7d](#)) because the additional  $\text{NO}_x$  further  
 409   accelerates the  $\text{RO}_x$  cycle (= accelerated VOC consumption).  $\text{NO}_2$  production was promoted,  
 410    $\text{NO}_2/\text{NO}_x$  ratio increased ([Figure 7e](#)), and  $\text{O}_3$  also increased ([Figure 6b](#)).

411

### 412      3.3.1.2 $\text{H}_2\text{O}_2/\text{HNO}_3$ indicator for identifying the $\text{O}_3$ sensitivity regime

413   The grayscale in [Figure 8](#) shows the  $\text{H}_2\text{O}_2/\text{HNO}_3$  ratio. [Sillman](#) (1995) first proposed the  
 414    $\text{H}_2\text{O}_2/\text{HNO}_3$  indicator that can identify the  $\text{O}_3$  sensitivity regime. This value is lower in the VOC-  
 415   limited region and higher in the  $\text{NO}_x$ -limited region. This is because, as mentioned above, the  
 416   main terminate products of the  $\text{RO}_x$  cycle are  $\text{H}_2\text{O}_2$  or  $\text{HNO}_3$  in  $\text{NO}_x$ -limited or VOC-limited  
 417   regions, respectively ([Sillman](#), 1995; [Sillman](#), 1999; [Sillman and He](#), 2002).

418   The distribution of monthly mean  $\text{H}_2\text{O}_2/\text{HNO}_3$  showed a trend of regime change from  
 419   urban to suburban areas ([Figure 8a](#)). However, it has been reported that the distribution of regime  
 420   boundary changes temporally and spatially (e.g., [Sillman](#), 1999; [Martill et al.](#), 2002; [Song et al.](#),  
 421   2010; [Lei et al.](#), 2007; [Kannari and Ohara](#), 2010). This is because the regime is determined by  
 422   multiple factors, not only the  $\text{NO}_x/\text{VOCs}$  emission ratio but also photochemical aging ([Sillman](#),  
 423   1999). Any polluted plumes immediately after being emitted are  $\text{NO}_x$ -rich and VOC-limited, but

424 over time,  $\text{NO}_x$  is removed by the process (R1, R2) and changes to  $\text{NO}_x$ -limited (*Milford et al., 1989*). However, if atmospheric mixing is weak and photochemical aging is slow, the transition  
425 from VOC-limited to  $\text{NO}_x$ -limited is delayed so that the VOC-limited region is expanded in the  
426 downwind suburbs (e.g., *Kleinman, 1994; Martilli et al., 2002; Spirig et al, 2002*).  
427

428

429 This is the reason why negative  $\text{O}_3$  sensitivity (VOC-limited) occurs in the suburban area  
430 circled by the dashed line in [Figure 6b](#).

431 In the July 26 13:00 case, the distribution of low  $\text{H}_2\text{O}_2/\text{HNO}_3$  corresponded to negative  
432  $\text{O}_3$  sensitivity (=VOC-limited), and high  $\text{H}_2\text{O}_2/\text{HNO}_3$  distribution corresponded to positive  $\text{O}_3$   
433 sensitivity (= $\text{NO}_x$ -limited) ([Figure 8b](#)). Furthermore, regime discrimination by the  $\text{H}_2\text{O}_2/\text{HNO}_3$   
434 index was successful not only in this one-hour value case but also when the region and period  
435 were expanded to include the nationwide and through July. Details for an evaluation of the  
436 versatility of the  $\text{H}_2\text{O}_2/\text{HNO}_3$  index and its best threshold are presented in Appendix A. In  
437 summary, depending on factors such as the rate of photochemical aging, the regime distribution  
438 may not conform to the general trend of VOC-limited in urban and  $\text{NO}_x$ -limited in suburbs (even  
439 suburbs can be VOC-limited).  $\text{H}_2\text{O}_2/\text{HNO}_3$  worked as a clear indicator that could discriminate  
440 such hourly changing regime boundaries and the best threshold was found as 0.5.  $\text{H}_2\text{O}_2/\text{HNO}_3$   
441 index is useful for predicting positive (where  $\text{H}_2\text{O}_2/\text{HNO}_3 > 0.5$ ) or negative (where  $\text{H}_2\text{O}_2/\text{HNO}_3$   
442 < 0.5)  $\text{O}_3$  sensitivity to emission changes in power plants.

443

444

445 3.3.2 Nighttime meteorology and atmospheric chemistry (atmospheric stability, effect  
446 of NO titration)

447

448 [Figures 9](#) and [10](#) are longitude–altitude cross-sections at 35.9°N and 35.5°N on July 26,  
449 2015, respectively (cut over the point of greater sensitivity in [Figure 6b](#)). Three-hourly snapshots  
450 are shown from 2:00 to 14:00 for (a)  $\text{NO}_x$  sensitivity, (b)  $\text{O}_3$  sensitivity and  $\text{H}_2\text{O}_2/\text{HNO}_3$  ratio,  
451 and (c)  $\text{PO}_3$  sensitivity, respectively, induced by additional power plant emissions. The  
452 sensitivity of  $\text{PO}_3$  (potential  $\text{O}_3$ ) ( $\Delta\text{PO}_3$ ) is defined by the following equation, which indicates the  
453 sensitivity of  $\text{O}_3$  concentration due to factors other than NO titration (i.e., chemical reaction

454 generation and advection). This indicator is based on the fact that  $O_3 + NO_2$  remains unchanged  
 455 even when  $O_3$  is decomposed in NO titration.

456

457 
$$\Delta[PO_3] = \Delta([O_3] + [NO_2] - 0.1 \times [NO_x]),$$

458

459 where  $[PO_3]$ ,  $[O_3]$ ,  $[NO_2]$ , and  $[NO_x]$  are their respective concentrations (ppb). 0.1, the  
 460 coefficient on  $NO_x$ , is the  $NO_2$  ratio in primary  $NO_x$  emissions, and the effect of primary  $NO_2$   
 461 emissions is removed in this term.

462 First, we focus on the area around Lake Kasumigaura, shown in cross-section (A). From  
 463 2:00 to 10:00 local time, additional  $NO_x$  from the thermal power plant in Kashima city titrated  
 464  $O_3$ , resulting in negative sensitivity ([Figures 9a and 9b](#)). During the night, the pollutants are  
 465 situated aloft in the upper part of the stable nighttime boundary layer. As the sun rose, the mixed  
 466 layer developed in the lower atmosphere, which resulted in positive  $O_3$  sensitivity in the  $NO_x$ -  
 467 limited region ([Figure 9b](#)). At 14:00,  $NO_x$  has been completely converted to  $HNO_3$ , the  
 468 terminated product of the  $RO_x$  cycle, so there is no sensitivity ([Figure 9a](#)). Approximately  
 469 140.8°E is the shoreline. The positive  $O_3$  sensitivity was lifted by the upwelling generated by the  
 470 land surface with higher surface temperatures and diffused significantly vertically within the  
 471 mixed layer ([Figure 9b](#)).

472 Next, we focus on the Tokyo Bay area shown in cross-section (B). As mentioned above,  
 473 additional  $NO_x$  from the power plants around Tokyo Bay titrated  $O_3$  during the night ([Figures](#)  
 474 [10a and 10b](#)). The plume was transported westward over the top of the stable nighttime boundary  
 475 layer, maintaining an emission altitude of 200–300 m, and thus, remained stagnant along the  
 476 terrain. As the sun rose, it diffused within the mixed layer with negative  $O_3$  sensitivity. The  
 477 negative  $O_3$  sensitivity at 14:00 can be mostly explained by VOC-limited chemistry ([Figures 10b](#)  
 478 and [10c](#)) because  $\Delta PO_3 \approx \Delta O_3$ , although there is still some contribution from the nighttime  
 479 titration. The distributions of negative  $O_3$  sensitivity and low  $H_2O_2/HNO_3$  values corresponded to  
 480 each ([Figure 10b](#)). This indicates that the  $H_2O_2/HNO_3$  indicator worked not only horizontally but  
 481 also vertically.

482 Conversely, focusing on the negative  $O_3$  sensitivity from the NO titration at night, the  
 483  $H_2O_2/HNO_3$  values are not lower ([Figures 9b and 10b](#)). This is because the NO titration process  
 484 contributes little to the terminated products of the  $RO_x$  cycle ( $HNO_3$  and  $H_2O_2$ ). This means that

485 negative O<sub>3</sub> sensitivity could occur if the NO titration process is dominant, even in areas  
486 identified as NO<sub>x</sub>-limited regions by the H<sub>2</sub>O<sub>2</sub>/HNO<sub>3</sub> ratio.  
487 This is consistent with what is described in *Sillman and He* (2002). To distinguish the effect of  
488 NO titration, it is necessary to use a different index than H<sub>2</sub>O<sub>2</sub>/HNO<sub>3</sub>, such as O<sub>3</sub>/NO<sub>y</sub> (*Sillman*  
489 *and He*, 2002).

490

491

492 **4 Conclusions**

493 The impact of all passenger cars shifting to BEV in Japan on O<sub>3</sub> concentrations in Kanto  
494 during summer was evaluated by sensitivity experiments using the regional meteorology–  
495 chemistry model NHM-Chem. The four sensitivity experiments were conducted under different  
496 conditions for on-road and upstream (thermal power plants and gas stations) emission changes.

497 The sensitivity of passenger cars in all BEV experiments indicated that daytime O<sub>3</sub>  
498 concentrations decreased over a wide area of the Kanto, resulting in a sensitivity of up to −5%  
499 (−4 ppbv) in the inland suburb following typical sea breeze transport patterns. Several previous  
500 studies that evaluated the impact of BEV penetration on air quality in other countries found that  
501 reduced NO<sub>x</sub> from vehicle exhaust reduces O<sub>3</sub> in suburbs but increases O<sub>3</sub> locally in urban,  
502 VOC-limited regions. In this study, however, daytime O<sub>3</sub> levels were reduced even in urban  
503 areas. That is because BEV shifting effectively reduced NMVOCs from the three evaporation  
504 sources: vehicle exhaust, vehicle evaporation, and gas station evaporation, and it is likely related  
505 to the Japanese context, where most passenger cars are gasoline-powered and fuel evaporative  
506 VOC emission regulations are relatively lax. These three sources contributed approximately  
507 4:3:3 to the reduction of NMVOC emissions on a mass basis, with alkanes from all sources  
508 contributing the most to the reduction. However, alkanes have a relatively low reactivity for O<sub>3</sub>  
509 formation. Therefore, on the basis of the ozone formation potential (OFP), which considers the  
510 reactivity of NMVOC species, it was estimated that the reduction of alkenes from fuel  
511 evaporation from passenger cars and gas stations, as well as aromatics from passenger car  
512 exhaust, contributed significantly to the reduction of O<sub>3</sub>. The contribution of the three NMVOC  
513 sources to OFP reduction was similar to that of the mass basis, with gasoline fuel evaporation  
514 contributing 60%, indicating its importance. Furthermore, it was found that only evaporation  
515 measures (without reducing passenger car exhaust) induced almost the same O<sub>3</sub> reduction effect  
516 in urban areas. Because a time lag in the real world before BEVs is widely adopted, it is  
517 presumed that introducing fuel evaporation measures (such as Stage 2) ahead of time will be  
518 effective for the early improvement of urban air quality. It was also suggested that NO<sub>x</sub> reduction  
519 is still important for reducing high O<sub>3</sub> concentrations over inland suburbs (NO<sub>x</sub>-limited region):  
520 BEV shifting is beneficial over the area.

521        The additional NO<sub>x</sub> emission from the thermal power plant due to BEV's nighttime  
522        charging contributed little to the monthly average of next daytime O<sub>3</sub> (−0.5% at most). This is  
523        because the plume emitted from point sources has different advection paths and chemical  
524        reaction rates depending on the daily meteorological field, and O<sub>3</sub> sensitivity becomes random.  
525        However, on some days, O<sub>3</sub> sensitivity can be higher, topically ± 5%. In these cases, additional  
526        pollutants from the thermal power plant during the night were stored in the upper part of the  
527        stable nighttime boundary layer and advected while maintaining an emission altitude of 200–300  
528        m, affecting the surface O<sub>3</sub> concentration at the arrival area as the mixed layer developed.

529        The concentration of O<sub>3</sub> tended to decrease (increase) in the plumes downwind of the  
530        power plant in urban (suburb) locations, which is consistent with the general distribution of O<sub>3</sub>  
531        sensitivity regime (VOC or NO<sub>x</sub>) change trend from urban to suburb. However, locations of  
532        regime boundaries change temporally and spatially, depending on factors such as the  
533        photochemical aging rate of the pollution plume. There were some cases of negative O<sub>3</sub>  
534        sensitivity (i.e., VOC-limited) in the suburbs in this study. We discovered that an H<sub>2</sub>O<sub>2</sub>/HNO<sub>3</sub>  
535        index with a threshold of 0.5 worked as a clear indicator to distinguish the spatial distributions of  
536        regime boundaries and was effective in predicting positive or negative O<sub>3</sub> sensitivity to  
537        additional NO<sub>x</sub> emissions from power plants. However, even in these regions determined to be  
538        NO<sub>x</sub>-limited by the H<sub>2</sub>O<sub>2</sub>/HNO<sub>3</sub> index, the O<sub>3</sub> sensitivity was negative if the NO titration process  
539        was dominant. To distinguish negative O<sub>3</sub> sensitivity due to the effect of NO titration, it is  
540        necessary to use a different index than H<sub>2</sub>O<sub>2</sub>/HNO<sub>3</sub>, such as O<sub>3</sub>/NO<sub>y</sub>.

541        The results in this study are similar to some of *Hata and Tonokura (2019)*, a previous  
542        study that evaluated the air quality impacts of ZEV deployment in Japan for the first time. This  
543        study additionally considers changes in the power plant emissions, which they did not consider,  
544        but the impacts are not very significant every month. It was discovered, however, that it could  
545        affect diurnal O<sub>3</sub> concentrations topically in space and time.

546        In this study, sensitivity experiments were conducted to evaluate the impact of a  
547        passenger car's BEV shifting. To predict a realistic future society, scenarios must be constructed  
548        based on more realistic assumptions, such as powertrain mix, including heavy-duty vehicles,  
549        charging patterns, power source mix, and power generation efficiency, and then evaluated in a  
550        model simulation. At that time, information on future powertrain mix for heavy-duty vehicles  
551        and future emission regulation for power plants is scarce, which will lead to uncertainties.

552 Furthermore, although we focused solely on O<sub>3</sub> in this study, it would be desirable to conduct an  
553 integrated assessment of other gaseous and particulate pollutants that have similar health effects,  
554 i.e., oxidative stress on the respiratory system.

555

556

## 557 **Appendix A: Evaluation of H<sub>2</sub>O<sub>2</sub>/HNO<sub>3</sub> ratio as an indicator of O<sub>3</sub> sensitivity regime**

558 We discuss the versatility and best thresholds for the H<sub>2</sub>O<sub>2</sub>/HNO<sub>3</sub> indicator here.

559 The threshold values of the indicator have been reported in several previous studies.

560 *Sillman and He (2002)* reported that H<sub>2</sub>O<sub>2</sub>/HNO<sub>3</sub> ≤ 0.2 ~ 0.4 at the 95th percentile value is the  
561 threshold for VOC-limited and H<sub>2</sub>O<sub>2</sub>/HNO<sub>3</sub> ≥ 0.7 ~ 3.1 for NO<sub>x</sub>-limited, based on model  
562 sensitivity experiments the United States. *Inoue et al. (2010b)* conducted a similar analysis to  
563 *Sillman and He (2002)* for five summer days in Japan and reported that the VOC-limited  
564 threshold is H<sub>2</sub>O<sub>2</sub>/HNO<sub>3</sub> ≤ 0.3. Multiple sensitivity experiments using chemical transport models  
565 are used to derive the threshold in these studies; NO<sub>x</sub> and VOC emissions are varied and O<sub>3</sub>  
566 sensitivity and corresponding H<sub>2</sub>O<sub>2</sub>/HNO<sub>3</sub> are statistically analyzed for all periods/grids. This  
567 study, however, did not conduct such multiple sensitivity experiments with finely tuned NO<sub>x</sub> and  
568 VOC parameters. As a result, the following methods were used to examine the versatility of the  
569 H<sub>2</sub>O<sub>2</sub>/HNO<sub>3</sub> indicator and to derive the best threshold value.

570 **Figure A1a** shows the correct judgment rate for the O<sub>3</sub> sensitivity regime when the  
571 H<sub>2</sub>O<sub>2</sub>/HNO<sub>3</sub> threshold is varied. The target is the grid data with O<sub>3</sub> ≥ 70 ppb and |ΔO<sub>3</sub>|  
572 (difference of O<sub>3</sub>, all BEV minus all BEV (PP unchanged)) (difference of O<sub>3</sub>, (2) All BEV  
573 experiment — (3) All BEV (PP unchanged) experiment) | ≥ 0.5 ppb, from 10:00 to 15:00 on  
574 July 1 to 31 in the national area shown in **Figure A1b**. In other words, develop a threshold that  
575 can accurately judge positive or negative O<sub>3</sub> sensitivity induced by additional NO<sub>x</sub> emissions  
576 from nationwide thermal power plants.

577 The light blue graph in **Figure A1a** shows the percentage of negative O<sub>3</sub> sensitivity in the  
578 data with H<sub>2</sub>O<sub>2</sub>/HNO<sub>3</sub> below the threshold (i.e., the percentage of the correct judgment of the  
579 VOC-limited). The lower (tougher) the threshold value is, the higher is the correct judgment rate.  
580 Furthermore, the higher the threshold value, the lower the correct judgment rate, converging to a  
581 probability of 1/2 (i.e., threshold meaningless state). The light-yellow graph in **Figure A1a**

582 depicts the percentage of positive O<sub>3</sub> sensitivity in the data with H<sub>2</sub>O<sub>2</sub>/HNO<sub>3</sub> above the threshold  
583 (i.e., the percentage of the correct judgment of the NO<sub>x</sub>-limited). For thresholds that are too small,  
584 this correct judgment rate will drop. For example, assume that we reduce H<sub>2</sub>O<sub>2</sub>/HNO<sub>3</sub> = 0.1 in  
585 [Figure 8b](#). You can image that the VOC-limited (negative O<sub>3</sub> sensitivity) can be filtered  
586 completely but the percentage of negative O<sub>3</sub> sensitivity would also be higher in the data above  
587 the threshold value (more miss judgment). Considering both (light blue and yellow), the best  
588 threshold value was derived as H<sub>2</sub>O<sub>2</sub>/HNO<sub>3</sub> = 0.5 for the target data in this study. Here, both  
589 NO<sub>x</sub>- and VOC-limited could be judged with a correct response rate of approximately 90%. It  
590 was determined to be adaptable even when the target area and period were expanded ([Figure](#)  
591 [A1a](#)).

592 We have discussed H<sub>2</sub>O<sub>2</sub>/HNO<sub>3</sub> indicator, but various other indicators have been  
593 proposed (e.g., O<sub>3</sub>/NO<sub>y</sub>, O<sub>3</sub>/NO<sub>z</sub>, O<sub>3</sub>/HNO<sub>3</sub>, (H<sub>2</sub>O<sub>2</sub> + ROOH)/HNO<sub>3</sub>, H<sub>2</sub>O<sub>2</sub>/NO<sub>z</sub>, (H<sub>2</sub>O<sub>2</sub> +  
594 ROOH)/NO<sub>z</sub>, H<sub>2</sub>O<sub>2</sub>/NO<sub>y</sub>, and (H<sub>2</sub>O<sub>2</sub> + ROOH)/NO<sub>y</sub>) ([Sillman and He, 2002](#)). It has been noted  
595 that in areas with high biogenic VOCs, the numerator should include organic peroxy radicals  
596 (ROOH) in addition to H<sub>2</sub>O<sub>2</sub> because the contribution of (R4) is larger in (R3, R4) ([Vermeuel et  
597 al., 2019](#)). It has also been pointed out that the denominator should be NO<sub>z</sub> or NO<sub>y</sub> because of  
598 the NO<sub>3</sub> ions in the HNO<sub>3</sub> transition between the gas and aerosol phases ([Martilli et al., 2002](#)).  
599 Considering these notes, we analyzed the same for (H<sub>2</sub>O<sub>2</sub> + ROOH)/NO<sub>z</sub>. As a result, the trend  
600 of (H<sub>2</sub>O<sub>2</sub> + ROOH)/NO<sub>z</sub> distribution was generally like that of H<sub>2</sub>O<sub>2</sub>/HNO<sub>3</sub>, which was also  
601 confirmed to work as a judgment index for the O<sub>3</sub> sensitivity regime (Figure S4). The best  
602 threshold value was estimated to be (H<sub>2</sub>O<sub>2</sub> + ROOH)/NO<sub>z</sub> = 0.35 (Figure S5).

603

604 **Acknowledgments**

605 The authors are thankful for Drs. Tazuko Morikawa and Hiroyuki Hagino of Japan Automobile  
606 Research Institute for providing PM2.5EI and useful comments on emission inventories and Ms.  
607 Natsumi Tanji of JMA for data processing. The authors are also thankful for Drs. Masayoshi  
608 Ishii, Akinori Takami, Seiji Sugata, and Tatsuya Nagashima of University of Tsukuba,  
609 Coorporative Graduate School Program and Dr. Akio Yamagami of MRI, Dr. Joseph Ching of  
610 University of Tottori, Mr. Tomoki Kajikawa, Ms. Rio Ishikawa, and Mr. Takuya Nakagawa of  
611 University of Tsukuba for useful discussion and comments on this study. This research was  
612 supported by Japanese Society for the Promotion of Sciences (JSPS) Grant-in-Aid for JSPS  
613 Fellows Grant Nos. JP21J22912 and Environmental Research and Technology Development  
614 Fund of the Environmental Restoration and Conservation Agency (ERCA)  
615 (JPMEERF20215003).

616 **Conflict of interest**

617 The authors declare no conflicts of interest relevant to this study.

618 **Data availability statement**

619 The raw data of REASv3.2.1 can be obtained from <https://www.nies.go.jp/REAS/> (last accessed:  
620 July 07, 2022). The screened data of AEROS are available at  
621 <https://soramame.env.go.jp/download> (last accessed: 7 July 2022).

622

623 **References**

- 624 **Amann, M.**, Derwent, D., Forsberg, B., Hänninen, O., Hurley, F., Krzyzanowski, M., Frank de  
625 Leeuw, Liu, S., Mandin, C., Schneider, J., Schwarze, P. and Simpson, D., (2008). Health  
626 risks of ozone from long-range transboundary air pollution. World Health Organization.  
627 Regional Office for Europe. <https://apps.who.int/iris/handle/10665/326496>
- 628 **Atkinson, R.** (1994). Gas-phase tropospheric chemistry of organic compounds. *Journal of*  
629 *Physical and Chemical Reference Data*. 2, 1-216

- 630 Atkinson, R. (1997). Gas-phase tropospheric chemistry of volatile organic compounds: 1.  
631 Alkanes and alkenes. *Journal of Physical and Chemical Reference Data*, 26(2), 215–290.  
632 <https://doi.org/10.1063/1.556012>
- 633 Atkinson, R. (2000). Atmospheric chemistry of VOCs and NO<sub>x</sub>. *Atmospheric Environment*, 34,  
634 2063–2101.
- 635 Carter, W. P. L. (1994). Development of ozone reactivity scales for volatile organic compounds.  
636 *Journal of the Air and Waste Management Association*, 44(7), 881–899.  
637 <https://doi.org/10.1080/1073161x.1994.10467290>
- 638 Carter, W. P. L. (2000). Documentation of the SAPRC-99 Chemical Mechanism for VOC  
639 Reactivity Assessment. Report to the California Air Resources Board, Contract 92-329  
640 and 95-308.
- 641 Central Environmental Council, (2017), Future Policy for Motor Vehicle Emission Reduction  
642 (Thirteenth Report), <https://www.env.go.jp/air/car/taisaku/index.html> (last accessed: 1  
643 July 2022) (in Japanese)
- 644 Central Environmental Council, (2022), Future Policy for Motor Vehicle Emission Reduction  
645 (Fourteenth Report), <https://www.env.go.jp/air/car/taisaku/index.html> (last accessed: 1  
646 July 2022) (in Japanese)
- 647 Enami, S., Hoffmann, M. R. and Colussi, A. J. (2008). Acidity enhances the formation of a  
648 persistent ozonide at aqueous ascorbate/ozone gas interfaces. *PNAS*, 105 (21), 7365–7369.  
649 [www.pnas.org/cgi/content/full/](http://www.pnas.org/cgi/content/full/)
- 650 Fukui, T., Kokuryo, K., Baba, T. and Kannari, A. (2014). Updating EAGrid2000 - Japan  
651 emissions inventory based on the recent emission trends. *Journal of Japan Society for  
652 Atmospheric Environment*, 49(2), 117–125. (in Japanese)
- 653 Giglio, L., Randerson, J.T. and Van Der Werf, G.R. (2013). Analysis of daily, monthly, and  
654 annual burned area using the fourth-generation global fire emissions database (GFED4).  
655 *Journal of Geophysical Research: Biogeosciences*, 118, 317–328.
- 656 Guenther, A., Karl, T., Harley, P., Wiedinmyer, C., Palmer, P. I. and Geron, C. (2006). Estimates  
657 of global terrestrial isoprene emissions using MEGAN (Model of Emissions of Gases and

- 658       Aerosols from Nature). *Atmospheric Chemistry and Physics* (Vol. 6). www.atmos-chem-  
659       phys.net/6/3181/2006/
- 660       **Hagino, H.**, Morikawa, T., Akiyama, K. and Sasaki, S. (2015). Volatile Organic Compounds and  
661       Air Quality Assessment Using Ozone Formation Potential in Refueling Loss Tests and  
662       Diurnal Breathing Loss Tests Using a Gasoline Fuel with Low Olefins. *Journal of Japan  
663       Society for Atmospheric Environment* (Vol. 50, Issue 6). (in Japanese)
- 664       **Hata, H.** and Tonokura, K. (2019). Impact of next-generation vehicles on tropospheric ozone  
665       estimated by chemical transport model in the Kanto region of Japan. *Scientific Reports*,  
666       9(1). <https://doi.org/10.1038/s41598-019-40012-y>
- 667       **Inoue, K.**, Yasuda, R., Yoshikado, H. and Higashino, H. (2010a). Spatial distribution of summer-  
668       time surface ozone sensitivity to NO<sub>x</sub> and VOC emissions for the Kanto area Part 1:  
669       Estimation by numerical simulations with two kinds of (larger and smaller) biogenic  
670       emission estimates. *Journal of Japan Society for Atmospheric Environment*, 45 (5). 183–  
671       194. (in Japanese)
- 672       **Inoue, K.**, Yoshikado, H. and Higashino, H. (2010b). Spatial distribution of summer-time surface  
673       ozone sensitivity to NO<sub>x</sub> and VOC emissions for the Kanto area Part2: Estimation based  
674       on the measurement of a photochemical indicator. *Journal of Japan Society for  
675       Atmospheric Environment*, 45 (5). 195–204. (in Japanese)
- 676       **Ito, A.**, Wakamatsu, S., Morikawa, T. and Kobayashi, S. (2021). 30 years of air quality trends in  
677       Japan. *Atmosphere*, 12(8). <https://doi.org/10.3390/atmos12081072>
- 678       **Kajino, M.**, Deushi, M., Sekiyama, T. T., Oshima, N., Yumimoto, K., Tanaka, T. Y., Ching, J.,  
679       Hashimoto, A., Yamamoto, T., Ikegami, M., Kamada, A., Miyashita, M., Inomata, Y.,  
680       Shima, S. I., Takami, A., Shimizu, A. and Hatakeyama, S. (2019). NHM-Chem, the Japan  
681       meteorological agency's regional meteorology – chemistry model: Model evaluations  
682       toward the consistent predictions of the chemical, physical, and optical properties of  
683       aerosols. *Journal of the Meteorological Society of Japan*, 97(2), 337–374.  
684       <https://doi.org/10.2151/JMSJ.2019-020>
- 685       **Kajino, M.**, Deushi, M., Sekiyama, T. T., Oshima, N., Yumimoto, K., Tanaka, T. Y., Ching, J.,  
686       Hashimoto, A., Yamamoto, T., Ikegami, M., Kamada, A., Miyashita, M., Inomata, Y.,

- 687 Shima, S.-I., Khatri, P., Shimizu, A., Irie, H., Adachi, K., Zaizen, Y. and Mikami, M.  
688 (2021). Comparison of three aerosol representations of NHM-Chem (v1.0) for the  
689 simulations of air quality and climate-relevant variables. *Geosci. Model Dev.*, 14, 2235–  
690 2264, <https://doi.org/10.5194/gmd-14-2235-2021>
- 691 Kannari, A., Tonooka, Y., Baba, T. and Murano, K. (2007). Development of multiple-species 1  
692 km × 1 km resolution hourly basis emissions inventory for Japan. *Atmospheric*  
693 *Environment*, 41(16), 3428–3439. <https://doi.org/10.1016/j.atmosenv.2006.12.015>
- 694 Kannari, A. and Ohara, T. (2010). Theoretical implication of reversals of the ozone weekend  
695 effect systematically observed in Japan. *Atmospheric Chemistry and Physics*, 10, 6765–  
696 6776
- 697 Ke, W., Zhang, S., Wu, Y., Zhao, B., Wang, S. and Hao, J. (2016). Assessing the future vehicle  
698 fleet electrification: The impacts on regional and Urban air quality. *Environmental*  
699 *Science and Technology*, 51(2), 1007–1016. <https://doi.org/10.1021/acs.est.6b04253>
- 700 Kleinman, L. I. (1994). Low and high NO<sub>x</sub> tropospheric photochemistry. *Journal of Geophysical*  
701 *Research*, Vol. 99, Issue D8.
- 702 Kobayashi, S., Ota, Y., Harada, Y., Ebita, A., Moriya, M., Onoda, H., Onogi, K., Kamahori, H.,  
703 Kobayashi, C., Endo, H., Miyaoka, K. and Kiyotoshi, T. (2015). The JRA-55 reanalysis:  
704 General specifications and basic characteristics. *Journal of the Meteorological Society of*  
705 *Japan*, 93(1), 5–48. <https://doi.org/10.2151/jmsj.2015-001>
- 706 Kurokawa, J. and Ohara, T. (2020). Long-term historical trends in air pollutant emissions in  
707 Asia: Regional Emission inventory in ASia (REAS) version 3. *Atmospheric Chemistry*  
708 *and Physics*, 20(21), 12761–12793. <https://doi.org/10.5194/acp-20-12761-2020>
- 709 Lei, W., Foy, B., Zavala, M., Volkamer, R. and Molina, L. T. (2007). Characterizing ozone  
710 production in the Mexico City Metropolitan Area: a case study using a chemical transport  
711 model, *Atmospheric Chemistry and Physics*, 7, 1347–1366
- 712 Li, N., Chen, J. P., Tsai, I. C., He, Q., Chi, S. Y., Lin, Y. C. and Fu, T. M. (2016). Potential  
713 impacts of electric vehicles on air quality in Taiwan. *Science of the Total Environment*,  
714 566–567, 919–928. <https://doi.org/10.1016/j.scitotenv.2016.05.105>

- 715 Martilli, A., Neftel, A., Favaro, G., Kirchner, F., Sillman, S. and Clappier, A. (2002). Simulation  
716 of the ozone formation in the northern part of the Po Valley. *Journal of Geophysical*  
717 *Research*, 107(D22), 8195. <https://doi.org/10.1029/2001JD000534>i
- 718 Milford, J. B., Russell, A. G. and McRae, G. J., (1989). A New Approach to Photochemical  
719 Pollution Control: Implications of Spatial Patterns in Pollutant Responses to Reductions  
720 in Nitrogen Oxides and Reactive Organic Gas Emissions. *Environ. Sci. Technol.* 1989, 23,  
721 1290-1301
- 722 Ministry of Land, Infrastructure and Transport, (2010), National Road and Street Traffic  
723 Conditions Survey (Road Traffic Census), <https://www.mlit.go.jp/road/census/h22-1/>,  
724 (last accessed: 5 July 2022) (in Japanese)
- 725 Ministry of Land, Infrastructure and Transport, urban bureau, (2012), Guidelines for the  
726 Installation of Charging Facilities in Parking Lots, etc. Guidelines for the Installation of  
727 Charging Facilities in Parking Lots, etc., <https://www.mlit.go.jp/common/000212869.pdf>,  
728 (last accessed: 5 July 2022) (in Japanese)
- 729 Ministry of Land, Infrastructure and Transport, (2012), Annual Report on Fuel Consumption of  
730 Automobiles. [https://www.mlit.go.jp/k-](https://www.mlit.go.jp/k-toukei/22/errata/kaitei/annual/pdf/new/22201200a00000_n.pdf)  
731 [toukei/22/errata/kaitei/annual/pdf/new/22201200a00000\\_n.pdf](https://www.mlit.go.jp/k-toukei/22/errata/kaitei/annual/pdf/new/22201200a00000_n.pdf), (last accessed: 5 July  
732 2022) (in Japanese)
- 733 Morikawa, T. (2017). Current status of Japanese emission inventory for PM2.5 and its problems.  
734 *Journal of Japan Society for Atmospheric Environment*, 52(3), A74–A78. (in Japanese)
- 735 Nakagawa, Y., Inoue, K., Yamada, H. and Tonokura, K. (2019). Assessment of Reduction of  
736 Fuel Evaporative Emission at the Time of Refueling on Air Quality in the Kanto Region,  
737 *Transactions of Society of Automotive Engineers of Japan*, 50(5) 1458-1462 (in Japanese).
- 738 Nopmongcol, U., Grant, J., Knipping, E., Alexander, M., Schurhoff, R., Young, D., Jung, J.,  
739 Shah, T. and Yarwood, G. (2017). Air Quality Impacts of Electrifying Vehicles and  
740 Equipment Across the United States. *Environmental Science and Technology*, 51(5),  
741 2830–2837. <https://doi.org/10.1021/acs.est.6b04868>
- 742 Ooka, R., Khiem, M., Hayami, H., Yoshikado, H., Huang, H. and Kawamoto, Y. (2011).  
743 Influence of meteorological conditions on summer ozone levels in the central Kanto area

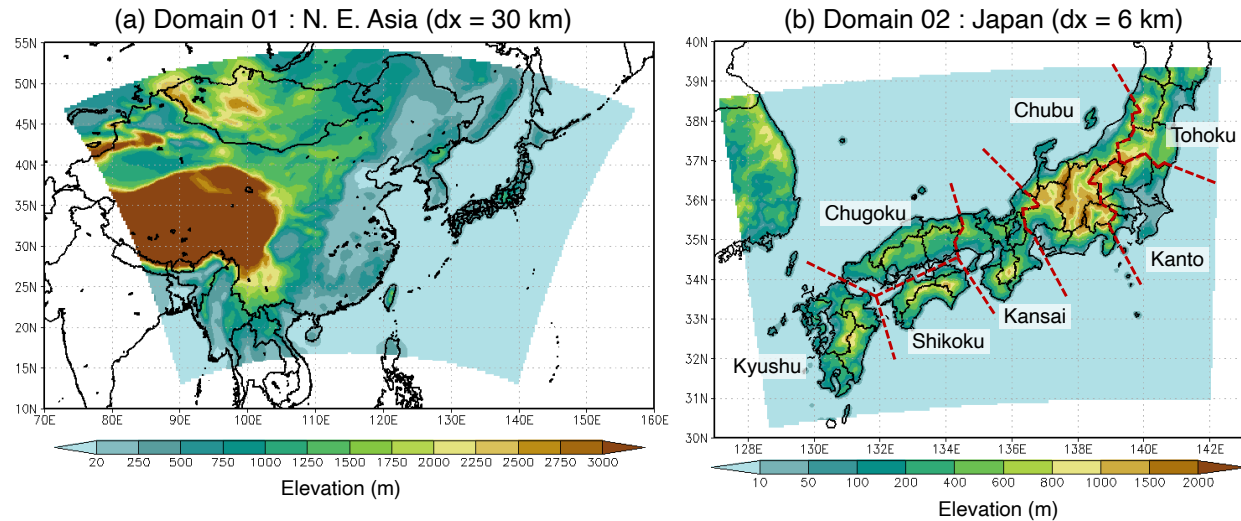
- 744 of Japan. *Procedia Environmental Sciences*, 4, 138–150.  
745 <https://doi.org/10.1016/j.proenv.2011.03.017>
- 746 **Pan, S.**, Roy, A., Choi, Y., Eslami, E., Thomas, S., Jiang, X. and Gao, H. O. (2019). Potential  
747 impacts of electric vehicles on air quality and health endpoints in the Greater Houston  
748 Area in 2040. *Atmospheric Environment*, 207, 38–51.  
749 <https://doi.org/10.1016/j.atmosenv.2019.03.022>
- 750 **Schnell, J. L.**, Naik, V., Horowitz, L. W., Paulot, F., Ginoux, P., Zhao, M., & Horton, D. E.  
751 (2019). Air quality impacts from the electrification of light-duty passenger vehicles in the  
752 United States. *Atmospheric Environment*, 208, 95–102.  
753 <https://doi.org/10.1016/j.atmosenv.2019.04.003>
- 754 **Schraufnagel, D. E.**, Balmes, J. R., Cowl, C. T., de Matteis, S., Jung, S. H., Mortimer, K., Perez-  
755 Padilla, R., Rice, M. B., Riojas-Rodriguez, H., Sood, A., Thurston, G. D., To, T., Vanker,  
756 A., & Wuebbles, D. J. (2019). Air Pollution and Noncommunicable Diseases: A Review  
757 by the Forum of International Respiratory Societies' Environmental Committee, Part 1:  
758 The Damaging Effects of Air Pollution. *Chest*, 155(2), 409–416. Elsevier Inc.  
759 <https://doi.org/10.1016/j.chest.2018.10.042>
- 760 **Sillman, S.** (1995). The use of NO<sub>y</sub>, H<sub>2</sub>O<sub>2</sub>, and HNO<sub>3</sub> as indicators for ozone- NO<sub>x</sub>-hydrocarbon  
761 sensitivity in urban locations. *Journal of Geophysical Research*, 100(D7), 14,175-14,188.
- 762 **Sillman, S.** (1999). The relation between ozone, NO<sub>x</sub> and hydrocarbons in urban and polluted  
763 rural environments. *Atmospheric Environment* (Vol. 33).
- 764 **Sillman, S. and He, D.** (2002). Some theoretical results concerning O<sub>3</sub>-NO<sub>x</sub>-VOC chemistry and  
765 NO<sub>x</sub>-VOC indicators. *Journal of Geophysical Research Atmospheres*, 107(22).  
766 <https://doi.org/10.1029/2001JD001123>
- 767 **Song, J.**, Lei, W., Bei, N., Zavala, M., de Foy, B., Volkamer, R., Cardenas, B., Zheng, J., Zhang,  
768 R. and Molina, L. T. (2010). Ozone response to emission changes: a modeling study  
769 during the MCMA-2006/MILAGRO Campaign. *Atmospheric Chemistry and Physics*,  
770 (Vol. 10). [www.atmos-chem-phys.net/10/3827/2010/](http://www.atmos-chem-phys.net/10/3827/2010/)

- 771 Soret, A., Guevara, M. and Baldasano, J. M. (2014). The potential impacts of electric vehicles on  
772 air quality in the urban areas of Barcelona and Madrid (Spain). *Atmospheric Environment*,  
773 99, 51–63. <https://doi.org/10.1016/j.atmosenv.2014.09.048>
- 774 Spirig, C., Neftel, A., Kleinman, L. I. and Hjorth, J. (2002). NO<sub>x</sub> versus VOC limitation of O<sub>3</sub>  
775 production in the Po valley: Local and integrated view based on observations. *Journal of*  
776 *Geophysical Research: Atmospheres*, 107(22). <https://doi.org/10.1029/2001JD000561>
- 777 Tager, I. B., Balmes, J., Lurmann, F., Ngo, L., Alcorn, S. and Künzli, N. (2005). Chronic  
778 exposure to ambient ozone and lung function in young adults. *Epidemiology*, 16(6), 751–  
779 759. <https://doi.org/10.1097/01.ede.0000183166.68809.b0>
- 780 Tajima, Y., Kato, S., Suthawaree, J. and Kajii, Y. (2010). Long-term measurement of various  
781 volatile organic compounds and air quality assessment using OH reactivity and ozone  
782 formation potential in sub-urban area of Tokyo. *Journal of Japan Society for*  
783 *Atmospheric Environment*, 45(2), 56–65.
- 784 Tang, Y., Dong, Y., Wittlin, S., Charman, S. A., Chollet, J., Chiu, F. C. K., Charman, W. N.,  
785 Matile, H., Urwyler, H., Dorn, A., Bajpai, S., Wang, X., Padmanilayam, M., Karle, J. M.,  
786 Brun, R. and Vennerstrom, J. L. (2007). Weak base dispiro-1,2,4-trioxolanes: Potent  
787 antimalarial ozonides. *Bioorganic and Medicinal Chemistry Letters*, 17(5), 1260–1265.  
788 <https://doi.org/10.1016/j.bmcl.2006.12.007>
- 789 Thompson, T., Webber, M. and Allen, D. T. (2009). Air quality impacts of using overnight  
790 electricity generation to charge plug-in hybrid electric vehicles for daytime use.  
791 *Environmental Research Letters*, 4(1). <https://doi.org/10.1088/1748-9326/4/1/014002>
- 792 Thompson, M. T., King, C. W., Allen, D. T. and Webber, M. E. (2011). Air quality impacts of  
793 plug-in hybrid electric vehicles in Texas: Evaluating three battery charging scenarios.  
794 *Environmental Research Letters*, 6(2). <https://doi.org/10.1088/1748-9326/6/2/024004>
- 795 Tonokura, K. and Hata, H (2020). Estimation of Evaporative Emissions from Parking  
796 and Refueling Processes of Gasoline Vehicles, *Journal of Japan Society for Atmospheric*  
797 *Environment*, 55(1), A1-A7

- 798    **Uchida, R.** (2016). Evaporative Emissions from Gasoline Vehicles-Review of Estimation for  
799        Evaporative Emissions in the United State. *JARI Research Journal*, 20160902 (in  
800        Japanese)
- 801    **Uchida, Y.**, Ishii, K., Ueno, H., Yokota, H., & Akiyama, K. (2013). An Emission Characteristics  
802        Study of Volatile Organic Compounds, Nitrogen Oxides and Fine Particulate Matter (PM  
803        2.5) from Motor-Vehicles in a Road Tunnel in 2010: Comparison with 2001. *J. Jpn. Soc.  
804        Atmos. Environ.*, 48 (3), 145–153(in Japanese)
- 805    **Vermeuel, M.** P., Novak, G. A., Alwe, H. D., Hughes, D. D., Kaleel, R., Dickens, A. F., Kenski,  
806        D., Czarnetzki, A. C., Stone, E. A., Stanier, C. O., Pierce, R. B., Millet, D. B. and  
807        Bertram, T. H. (2019). Sensitivity of Ozone Production to NO<sub>x</sub> and VOC Along the Lake  
808        Michigan Coastline. *Journal of Geophysical Research: Atmospheres*, 124(20), 10989–  
809        11006. <https://doi.org/10.1029/2019JD030842>
- 810    **Yamada, H.**, Inomata, S. and Tanimoto, H. (2015a). Evaporative emissions in three-day diurnal  
811        breathing loss tests on passenger cars for the Japanese market. *Atmospheric Environment*,  
812        107, 166–173. <https://doi.org/10.1016/j.atmosenv.2015.02.032>
- 813    **Yamada, H.**, Inomata, S. and Tanimoto, H. (2015b). Refueling emissions from cars in Japan:  
814        Compositions, temperature dependence and effect of vapor liquefied collection system.  
815        *Atmospheric Environment*, 120, 455–462.  
816        <https://doi.org/10.1016/j.atmosenv.2015.09.026>
- 817    **Zhang, J.J.**, Wei, Y. and Fang, Z. (2019). Ozone Pollution: A Major Health Hazard Worldwide.  
818        *Frontiers in Immunology*, 10, 2518.
- 819
- 820    **References from Supporting Information**
- 821    **Clarke, A. D.**, Owens, S. R. and Zhou, J. (2006). An ultrafine sea-salt flux from breaking waves:  
822        Implications for cloud condensation nuclei in the remote marine atmosphere. *Journal of  
823        Geophysical Research*, 111, D06202, 14 pp.

- 824 Deushi, M. and Shibata, K. (2011). Development of an MRI Chemistry-Climate Model ver.2 for  
825 the study of tropospheric and stratospheric chemistry. *Papers in Meteorology and*  
826 *Geophysics*, 62, 1-46.
- 827 Han, Z., Ueda, H., Matsuda, K., Zhang, R., Arao, K., Kanai, Y. and Hasome, H. (2004). Model  
828 study on particle size segregation and deposition during Asian dust events in March 2002.  
829 *Journal of Geophysical Research*, 109, D19205, 22 pp.
- 830 Tanaka, T., Y., Orito, K., Sekiyama, T. T., Shibata, K., Chiba, M. and Tanaka, H. (2003).  
831 MASINGAR, a global tropospheric aerosol chemical transport model coupled with  
832 MRI/JMA98 GCM: Model description. *Papers in Meteorology and Geophysics*, 53(4),  
833 119-138.
- 834 Tanaka, T. Y. and Ogi, A. (2017). Update of Japan Meteorological Agency's global mineral dust  
835 operational forecast model. *Sokkou-Jihou*, 84, 109-128 (in Japanese).
- 836 Yumimoto, K., Tanaka, T., Y., Oshima, N. and Maki, T. (2017). JRAero: the Japanese  
837 Reanalysis for Aerosol v1.0. *Geoscientific Model Development*, 10, 3225-3253.
- 838
- 839

840

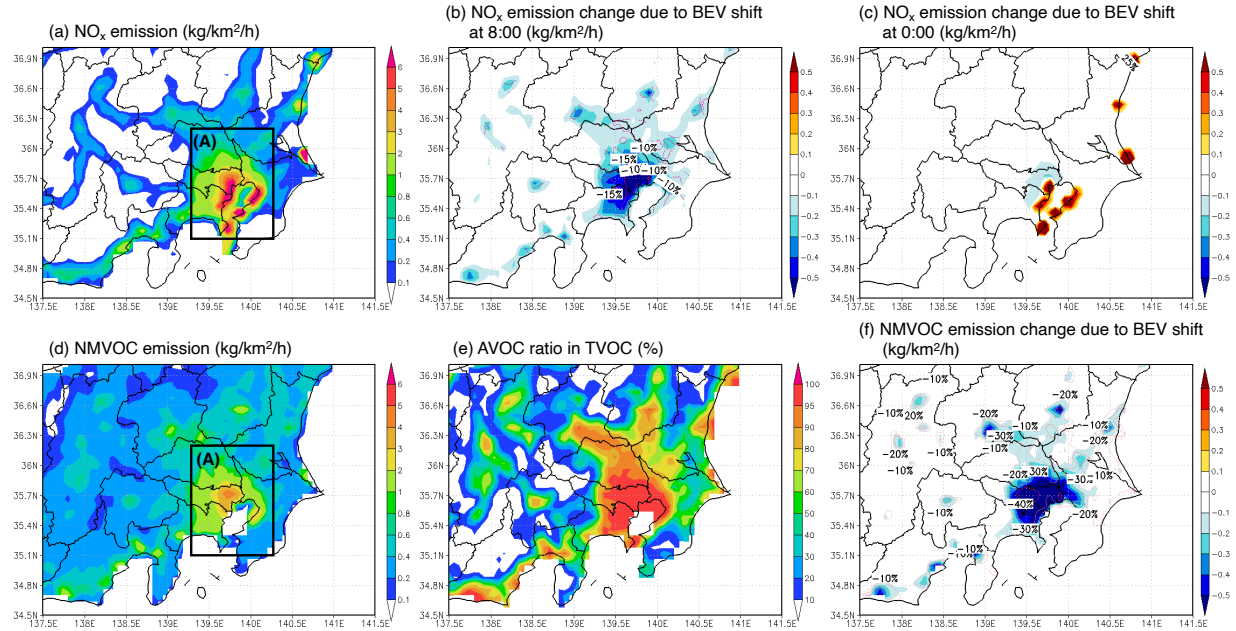


841

842 **Figure 1.** Model domains in this study. (a) Terrestrial elevations of domain 01 (North East Asia,  
843  $dx = 30 \text{ km}$ ). (b) Same as (a) but for domain 02 (Japan,  $dx = 6 \text{ km}$ ).

844

845

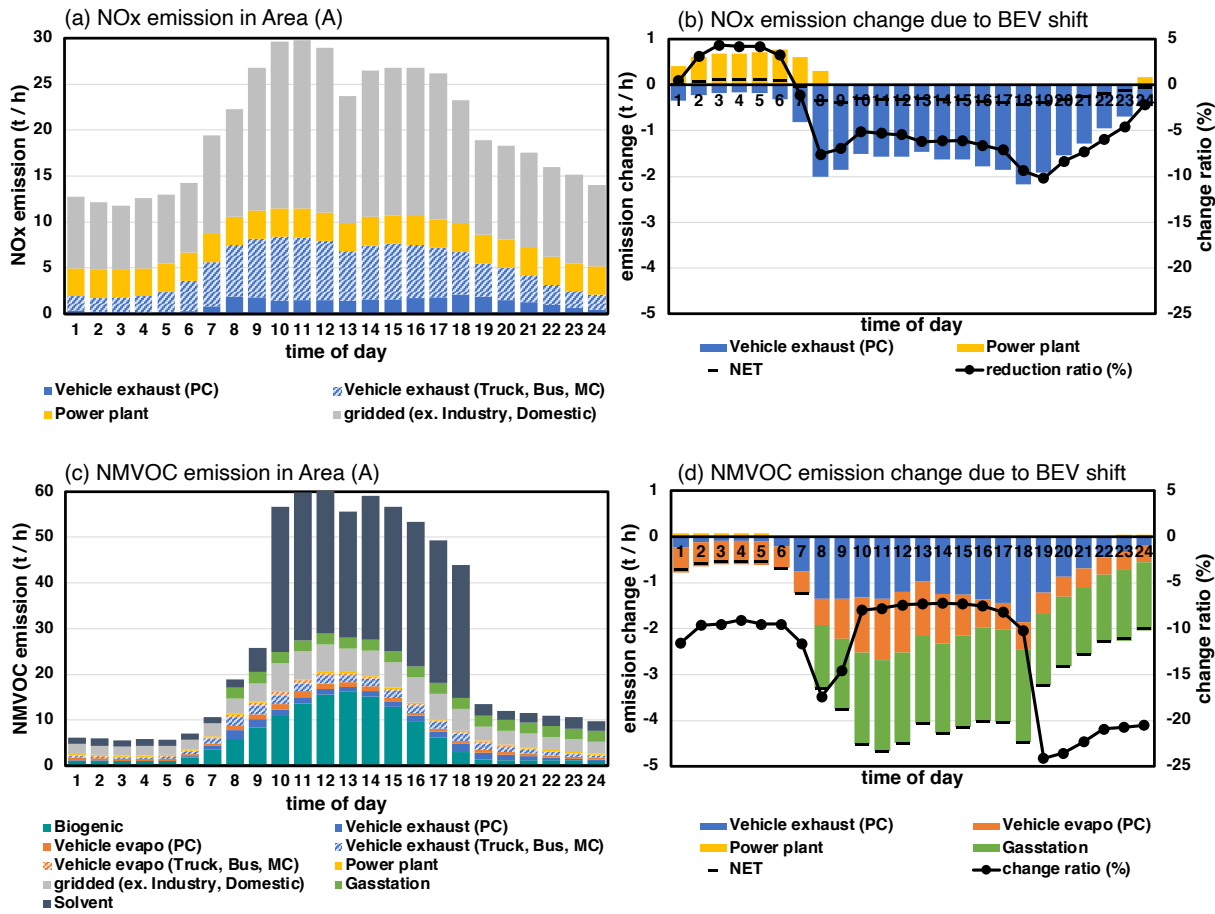


846

847 **Figure 2.** Monthly mean NO<sub>x</sub> and NMVOC emissions in the BASE experiment and their  
 848 changes in all BEV experiments in Kanto in July 2015: (a) NO<sub>x</sub> emission flux in the BASE  
 849 experiment, (b) changes in NO<sub>x</sub> flux at 8:00 a.m. local time, (c) changes in NO<sub>x</sub> flux at 0:00 a.m.  
 850 local time, (d) NMVOC emission flux in the BASE experiment, (e) anthropogenic ratio to the  
 851 total NMVOC emission flux in the BASE experiment, and (f) changes in NMVOC flux due to  
 852 BEV shift. The major emission source area is framed (A).

853

854



855

856 **Figure 3.** Diurnal variation of the monthly and areal mean (a) NOx and (b) NMVOC emissions  
 857 and (c, d) their emission changes in all BEV experiments in the area (A) ([Figure 2](#)). Weekdays  
 858 and weekends are weighted by the number of days in July.

859

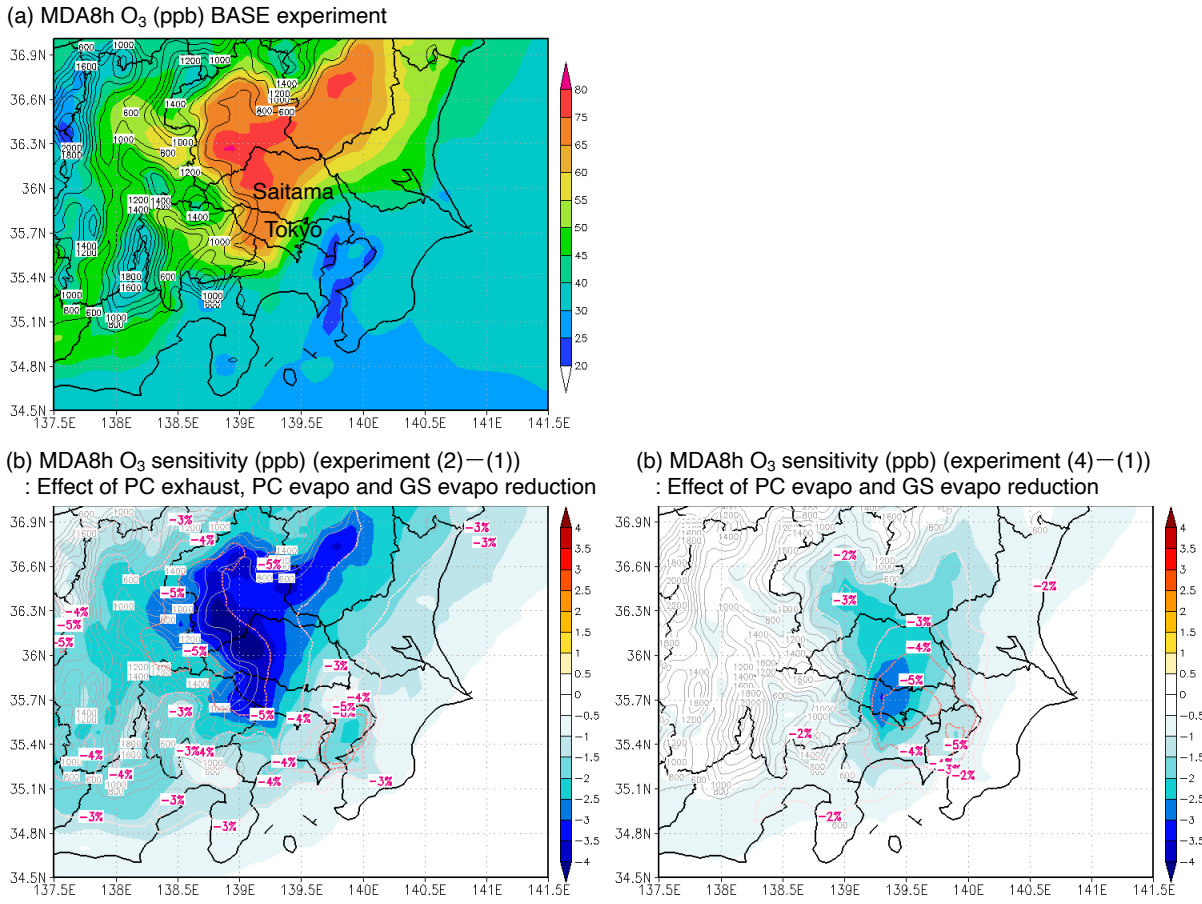
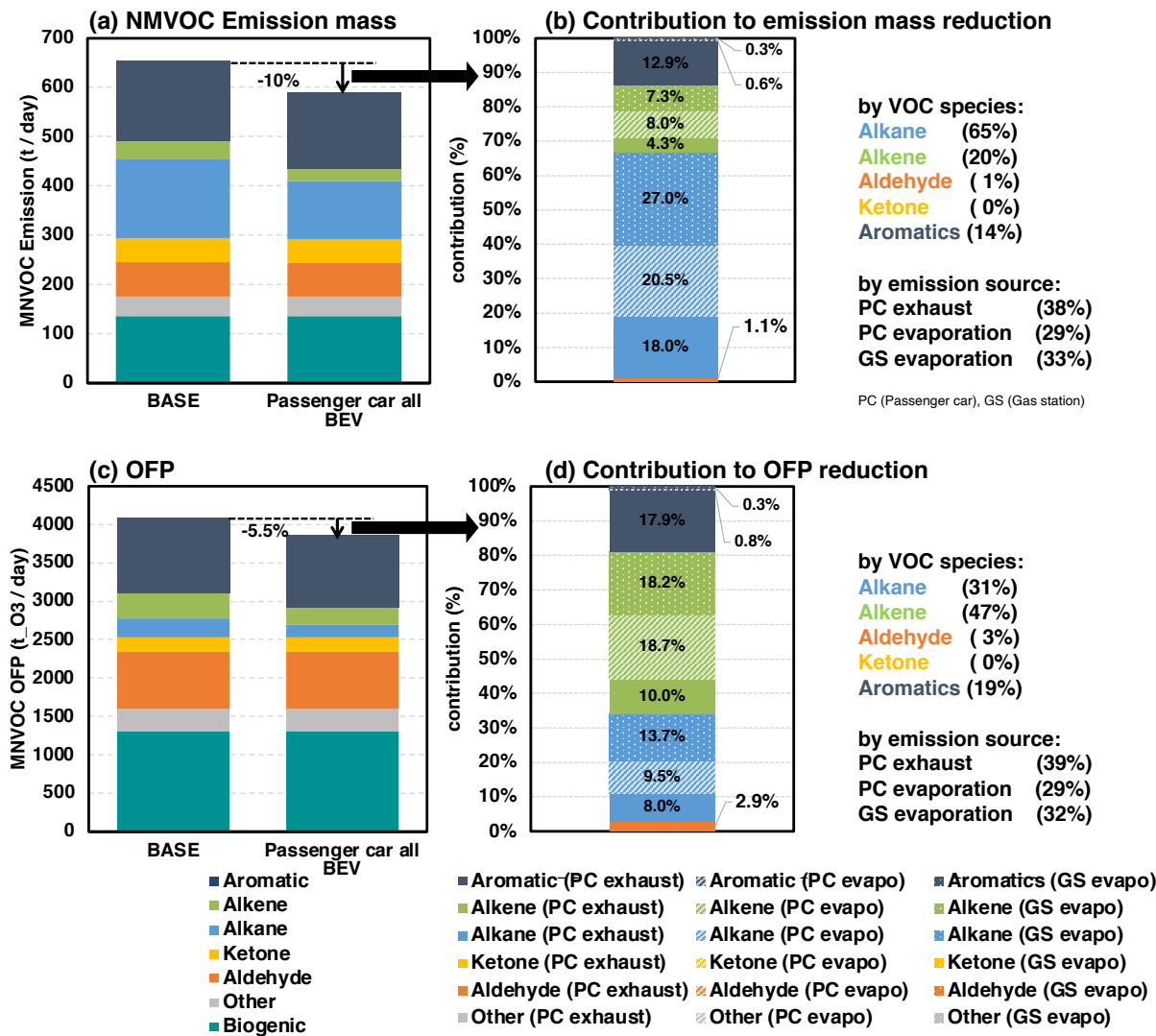


**Figure 4.** Monthly mean concentrations of MDA8h O<sub>3</sub> in July 2015: (a) BASE experimental result, (b) sensitivity of all BEV experiment, and (c) sensitivity of Evapo reduction experiment (c), respectively. Numbers in the title of each panel correspond to the sensitivity experiment, as listed in [Table 1](#). The thin black or gray contours indicate terrestrial elevation (m). The pink contours of (b) and (c) indicate the change ratio of O<sub>3</sub> concentration (%).



867

868 **Figure 5.** Monthly and areal total emissions of NMVOC (a) mass and (c) ozone formation  
 869 potential (OFP) with the contributions of VOC speciation in the BASE experiment and their  
 870 changes in all BEV experiments in the area (A) ([Figure 2](#)). 5b and 5d show the contribution of  
 871 each VOC specie and emission source to the reductions of 5a and 5c, respectively. OFP is  
 872 NMVOC emissions weighted by maximum incremental reactivity (MIR). The values of MIR  
 873 based on the SAPRC-99 speciation ([Carter, 2000](#)) are shown in Table S2.

874

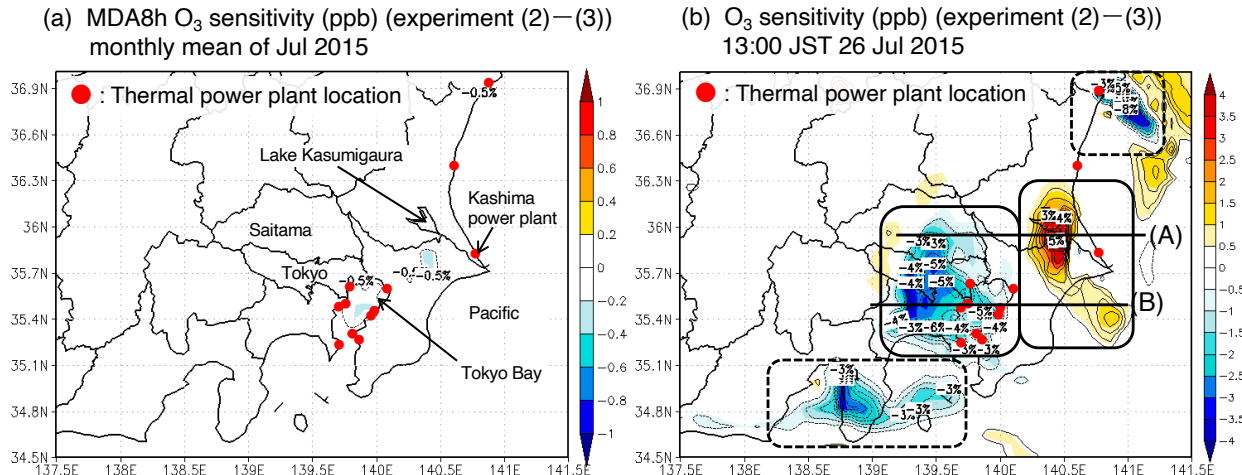
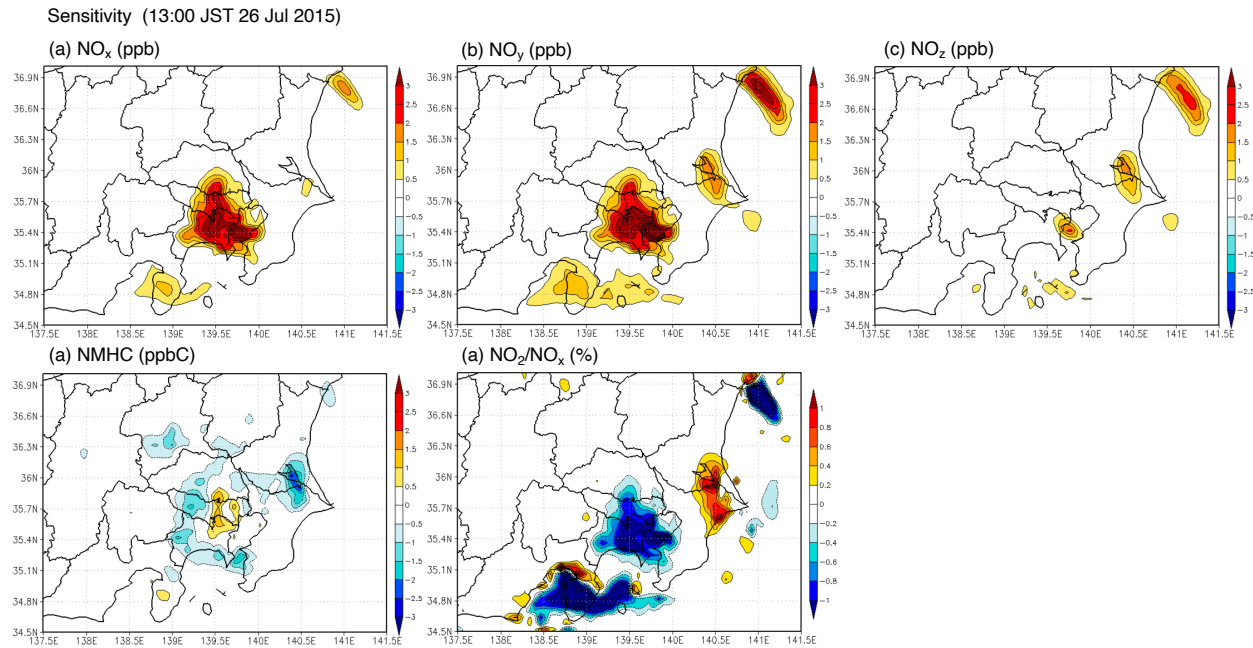


**Figure 6.** The sensitivity of the next daytime O<sub>3</sub> concentration is due to additional thermal power plant emission for BEV night charging. MDA8h O<sub>3</sub> of July average (a) and the case of 14:00 JST 26 July (b). Numbers in the title of each panel correspond to the sensitivity experiment, as listed in [Table 1](#). Thermal power plant locations are indicated by red dots. (A) and (B) each passes through a point of high sensitivity. In the region enclosed with the solid line (b), the positive and negative sensitivity of O<sub>3</sub> is consistent with the general O<sub>3</sub> sensitivity regime (VOC-limited in urban and NO<sub>x</sub>-limited in the suburb). In the region enclosed with the dashed line (b), O<sub>3</sub> sensitivity is not consistent with the general sensitivity regime.

884

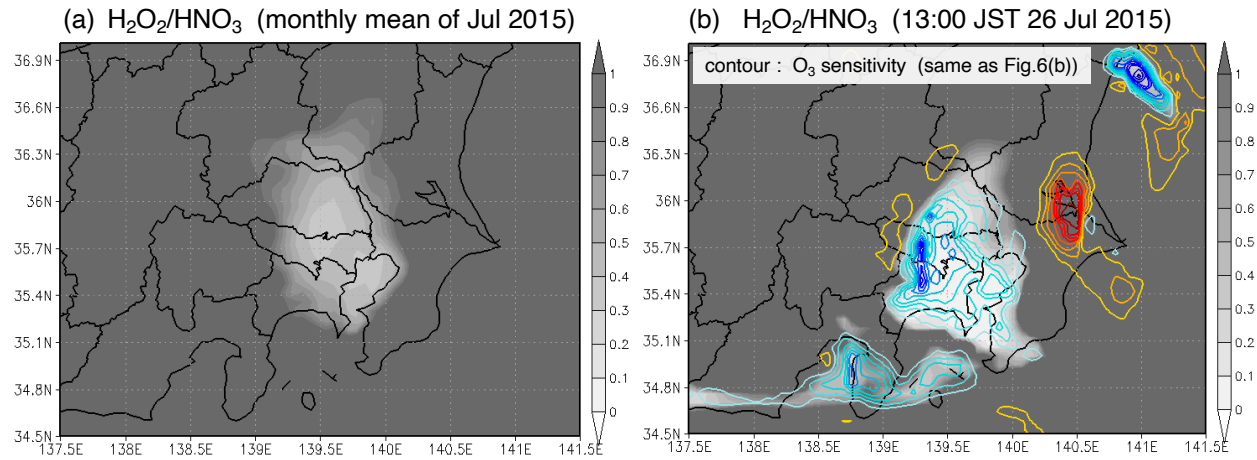


885

886 **Figure 7.** The sensitivity of next daytime NO<sub>x</sub>, NO<sub>y</sub>, NO<sub>z</sub>, NMHC concentration, and NO<sub>2</sub>/NO<sub>x</sub>  
 887 ratio due to the additional thermal power plant emission for BEV night charging (the case of  
 888 14:00 JST 26 July).

889

890

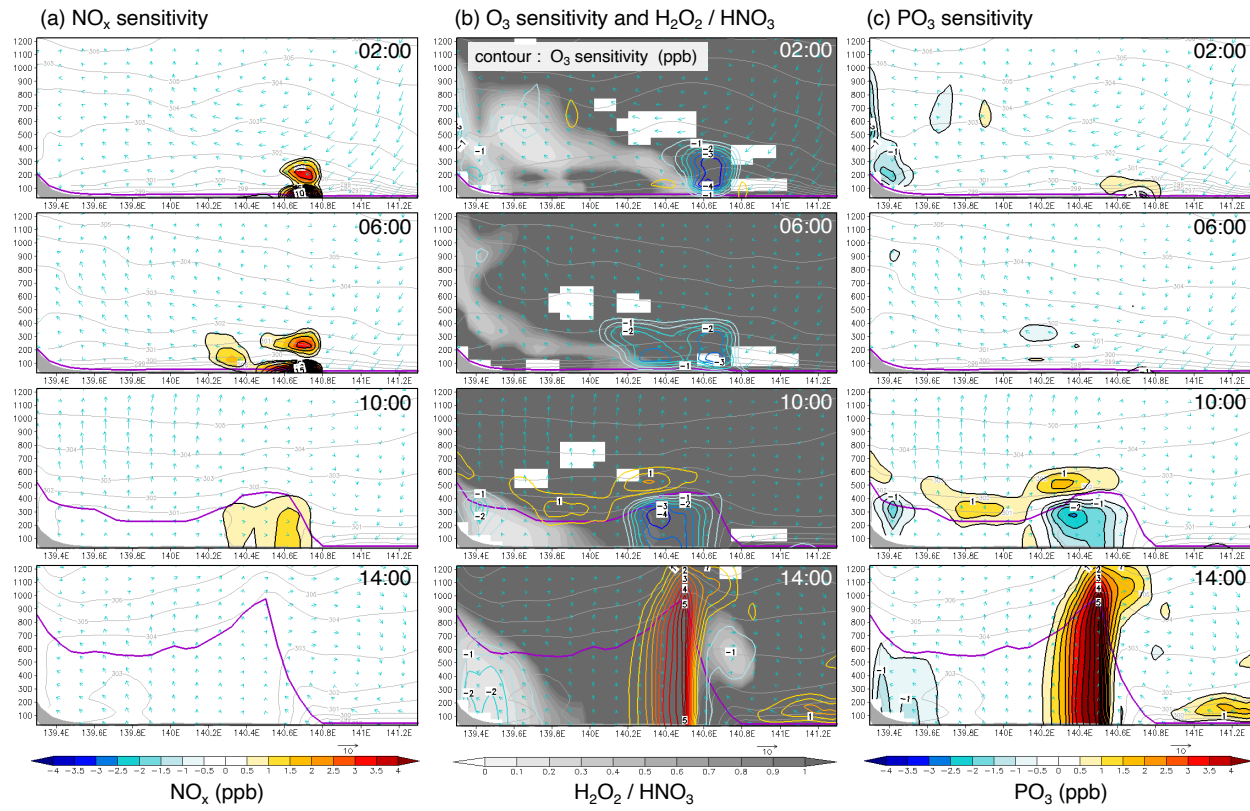


891

892 **Figure 8.** The distribution of  $\text{H}_2\text{O}_2/\text{HNO}_3$ . July average (a) and the case of 14:00 JST 26 July (b).  
893 The contour of (b) indicates  $\text{O}_3$  sensitivity, as shown in [Figure 6b](#).

894

Lon-alt cross section at 35.9° N in 26 Jul 2015



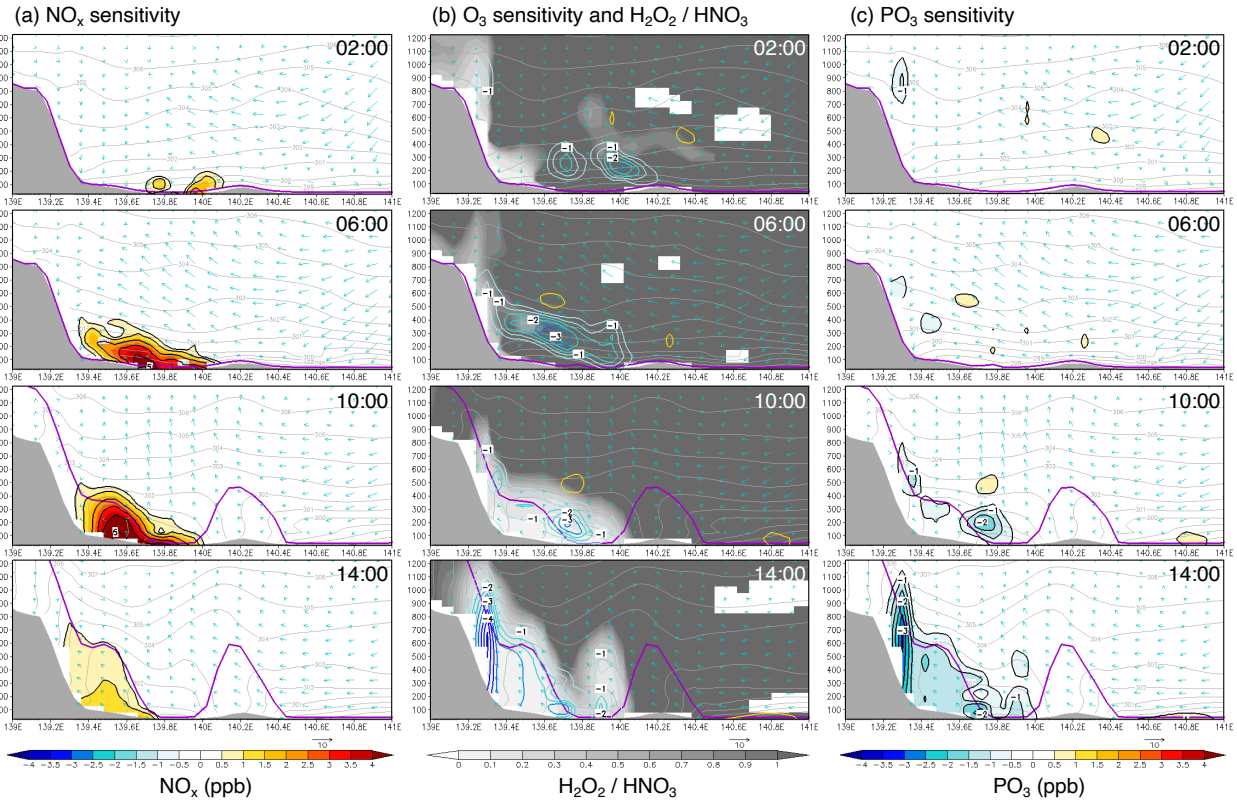
895

**Figure 9.** Longitude–altitude cross-section at 35.9°N shown in [Figure 6b-line \(A\)](#): (a) NO<sub>x</sub> sensitivity, (b) PO<sub>3</sub> sensitivity, and (c) O<sub>3</sub> sensitivity and H<sub>2</sub>O<sub>2</sub>/HNO<sub>3</sub>, respectively. The Y-axis indicates the height above sea level (m). The gray contours indicate the potential temperature. The purple line indicates mixed layer altitude. The mixed layer altitude here is the lowest altitude in the vertical profile of the virtual potential temperature of each layer of the model that exceeds the virtual potential temperature of the lowest layer of the atmosphere. The H<sub>2</sub>O<sub>2</sub>/HNO<sub>3</sub> ratio has an error value (infinity; white blank) when HNO<sub>3</sub> is extremely low in [Figure 9b](#).

903

904

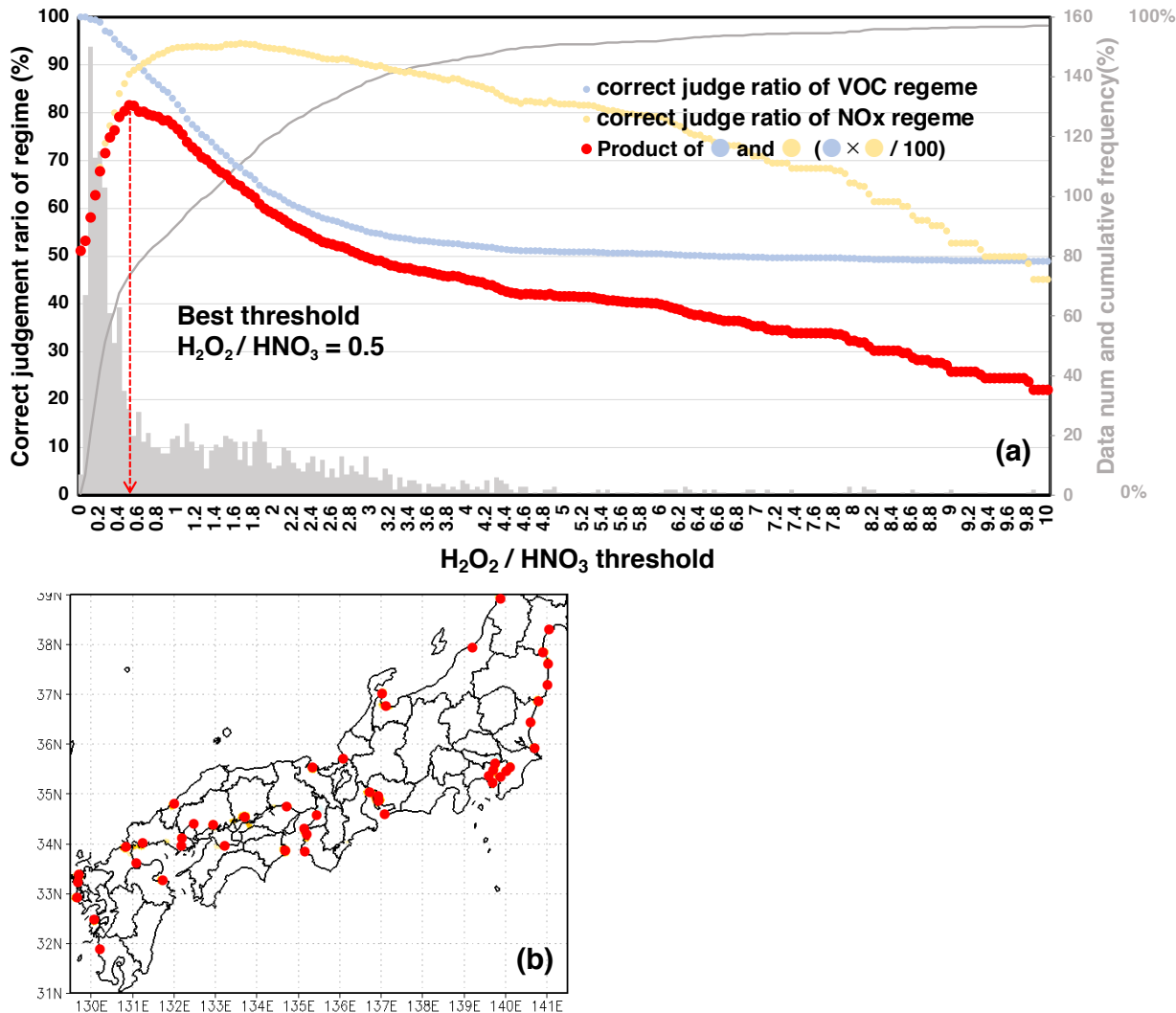
Lon-alt cross section at 35.5° N in 26 Jul 2015



905

906 **Figure 10.** Same as Figure 9 but at 35.5°N shown in Figure 6b-line (B).

907



908

**Figure A1.** The correct judgment ratio of the O<sub>3</sub> sensitivity regime (NO<sub>x</sub>- or VOC-limited) when the H<sub>2</sub>O<sub>2</sub>/HNO<sub>3</sub> threshold is varied. The target is the grid data with O<sub>3</sub> ≥ 70 ppb and |ΔO<sub>3</sub>| ≥ 0.5 ppb from 10:00 to 15:00 on July 1 to 31 in the national area shown in (b). The histogram of H<sub>2</sub>O<sub>2</sub>/HNO<sub>3</sub> corresponding to them is the right vertical axis in (a). In (a), the light blue graph shows the percentage of negative O<sub>3</sub> sensitivity in the data with H<sub>2</sub>O<sub>2</sub>/HNO<sub>3</sub> below the threshold (i.e., the percentage of the correct judgment of the VOC-limited). The light-yellow graph shows the percentage of positive O<sub>3</sub> sensitivity in the data with H<sub>2</sub>O<sub>2</sub>/HNO<sub>3</sub> above the threshold (i.e., the percentage of the correct judgment of the NO<sub>x</sub>-limited). The red graph is the product of light blue and light-yellow.

918

919

920 **Table 1.** Simulation experimental cases in this study. Emission factors for the sensitivity  
 921 experiments (2, 3, and 4) to base experiment (1) for each emission source of O<sub>3</sub> precursors.

Emission source	O <sub>3</sub> prediction	(1) BASE	(2) all BEV	(3) all BEV (PP <sup>b</sup> unchanged)	(4) Evapo reduce
Passenger car exhaust	NO <sub>x</sub> , NMVOC, CO	1	0	0	1
Passenger car evaporation (RL, HSL, DBL)	NMVOC	1	0	0	0
Gas station evaporation	NMVOC	1	0.2	0.2	0.2
PP <sup>b</sup>	mainly NO <sub>x</sub>	1	approximately 1.25 <sup>a</sup> at 23:00~8:00	1	1

922 a. Reference Figure S1.

923 b. Thermal power plant.

924

925

926 **Table 2.** Statistical comparison of the model BASE experimental result and observation data for  
 927 O<sub>3</sub> and MDA8h O<sub>3</sub> in July 2015.

	Region	Period	N	Obs. mean	Sim. mean	R	MB	NMB (%)
O <sub>3</sub> (ppb)	Kanto	July 2015	31	28.2	25.4	0.66	-2.7	-9.7
MDA8h O <sub>3</sub> (ppb)	(1 region)	(31 days)	31	44.8	46.4	0.79	1.6	3.6
O <sub>3</sub> (ppb)	Japan all	July 2015	869	24.6	25.5	0.32	0.9	3.8
MDA8h O <sub>3</sub> (ppb)	(869 grid)	(monthly mean)	869	37.2	40.3	0.56	3.1	8.4

928

929